T H E U N I V E R S I T Y O F M I C H I G A N

COLLEGE OF ENGINEERING

Department of Nuclear Engineering

Laboratory For Fluid Flow and Heat Transport Phenomena

Technical Report No. 13

CAVITATION DAMAGE TESTS OF STRESSED SPECIMENS WITH MERCURY IN A VENTURI

Lawrence L. Barinka

Frederick G. Hammitt

M. John Robinson

R. D. Pehlke

C. A. Siebert

ORA Project 03424

under contract with:

NATIONAL AERONAUTICS AND SPACE ADMINISTRATION

GRANT NO. NsG-39-60

WASHINGTON 25, D. C.

administered through:

OFFICE OF RESEARCH ADMINISTRATION ANN ARBOR

November 1963

ACKNOWLEDGMENTS

In addition to the authors, the following faculty and research personnel of The University of Michigan made significant contributions to the present investigation: Messrs. H. M. Ring, O. N. Senturk, V. A. Biss, E. D. Shippey, and Wm. Glesner.

ABSTRACT

Cavitation damage tests of stainless steel specimens under tensile stress were conducted in the venturi cavitation damage facility at The University of Michigan. Specimens were tested in mercury at a throat velocity of 34 ft/sec for 90 hours, and at applied tensile stresses of up to about 1.3 times the tensile yield strength of the material tested, i.e., to about 2/3 of the ultimate tensile strength.

The yield and ultimate strengths of the stainless steel specimens* were observed to decrease from damage due to cavitation alone, and for cavitation in combination with an applied tensile stress. The applied stress had only a small effect on the development of cavitation damage but did affect the gross weakening of the test specimens from a given quantity of cavitation damage in terms of mean depth of penetration.

---

* As used in this report, these parameters are always based on the original cross-sectional area.

TABLE OF CONTENTS

TABLE OF CONTENTS (CONT'D)

LIST OF TABLES

LIST OF FIGURES

LIST OF FIGURES (CONT'D)

1.0 INTRODUCTION

Cavitation is an important phenomenon because of its effects on the fluid-dynamic performance of a flowing system, and the resulting damaging of materials. The present project is an effort to investigate this phenomenon, using both water and liquid metals, in the venturi cavitation facility of The University of Michigan's Nuclear Engineering Department.

A considerable amount of data has already been reported under the U-M investigation[2,3,4] on the venturi damage tests of various materials in both water and mercury (at room temperature), and future tests are planned for liquid metal runs at temperatures up to 1000 ^{o}F. Although these tests were conducted on unstressed specimens, components of a flowing system exposed to cavitation are generally under stress, e.g. the centrifugal and bending stresses acting on an impeller. Thus it was thought desirable to test specimens under stress in the mercury* cavitation facility. It was expected that such tests would lead to:

i) a more fundamental understanding of the mechanism of cavitation damage in rotating pumping machinery, and

ii) an increased ability to predict damage to flow components in various fluids.

The main questions hopefully to be answered by such tests are:

i) How does the imposed stress pattern affect the development of cavitation damage?

---

* Mercury provides an "accelerated" cavitation damage test so that significant results would appear much more rapidly with this fluid than with water.

ii) What effect does cavitation alone, and cavitation in combination with an applied stress, have on the mechanical strength properties of the material tested?

iii) Does a room temperature specimen, stressed to any level, creep appreciably while under the attack of cavitation, due to the repeated, but local, exceeding of the yield (or even ultimate) stress on the surface?

It is the purpose of this report to discuss the method used for preliminary tests of specimens in a cavitating regime under stress, and to present the results of these tests.

2.0 EQUIPMENT AND PROCEDURE

2.1 Test Facility

The test facility has been previously described in detail[1,2,3]; however, a brief summary of the major items of equipment will be given here for convenience.

The over-all test facility is shown schematically in Figure 1. The closed loop consists of a venturi test section, a flow measuring venturi, two throttle valves, and approximately 20 feet of $1\frac{1}{2}$ inch, Schedule 40, stainless steel pipe. It is powered by an overhung, "sump-type", centrifugal pump capable of producing a head rise in mercury of about 40 feet of fluid at a flow rate of about 40 GPM. The restricted size of the loop is due to the desire to test high temperature liquid metals in the same facility*.

- -

* The facility is presently being converted to enable tests to be conducted with a lead-bismuth alloy at temperatures up to 1000 ^{o}F.

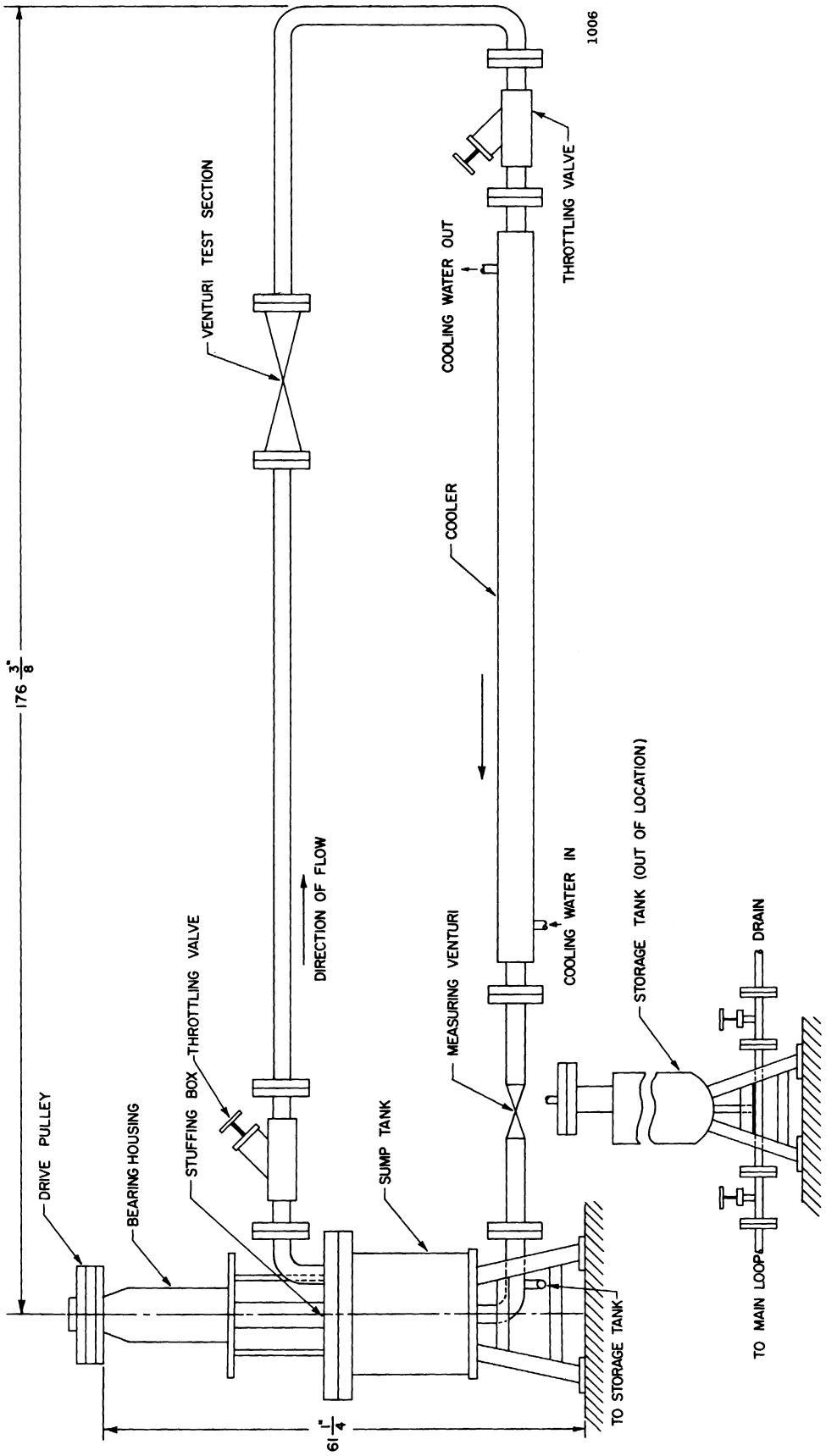

Figure 1 Schematic Drawing of Test Facility.

The throttle valves are located upstream and downstream of the venturi, so that the venturi throat pressure can be varied, while maintaining constant pump head and flow. Static pressures at various tap positions are measured by precision Heise gages. All pressure instrument lines lead into a common manifold through simple on-off toggle valves; the manifold is similarly connected to Heise gages of appropriate range. Flow rate is measured with a mercury manometer, utilizing the previously mentioned metering venturi.

Previously reported[2,3,4] tests, on unstressed specimens in water and mercury, used a plexiglas venturi (Figure 2), having a 6^{o}-included angle nozzle and diffuser, separated by a cylindrical throat of 0.51-inch diameter and 2.35-inch length. Cavitation initiates at the downstream end of the cylindrical throat. Its termination point in the diffuser, determined visually, is adjusted primarily by the downstream throttling valve. For ordinary damage tests, two unstressed specimens are inserted into the cavitation field through the wall of the venturi (Figure 2).

2.2 Tension Test Equipment

After reviewing several possible methods for testing specimens under stress in the cavitation facility, the following arrangement was adopted. A single specimen, gripped at both ends, extends across the entire fluid stream in the diffuser region of the venturi, approximately at the axial location of unstressed specimens (Figure 2). An external tensile load is applied to the specimen by a heavy clamp external to the venturi.

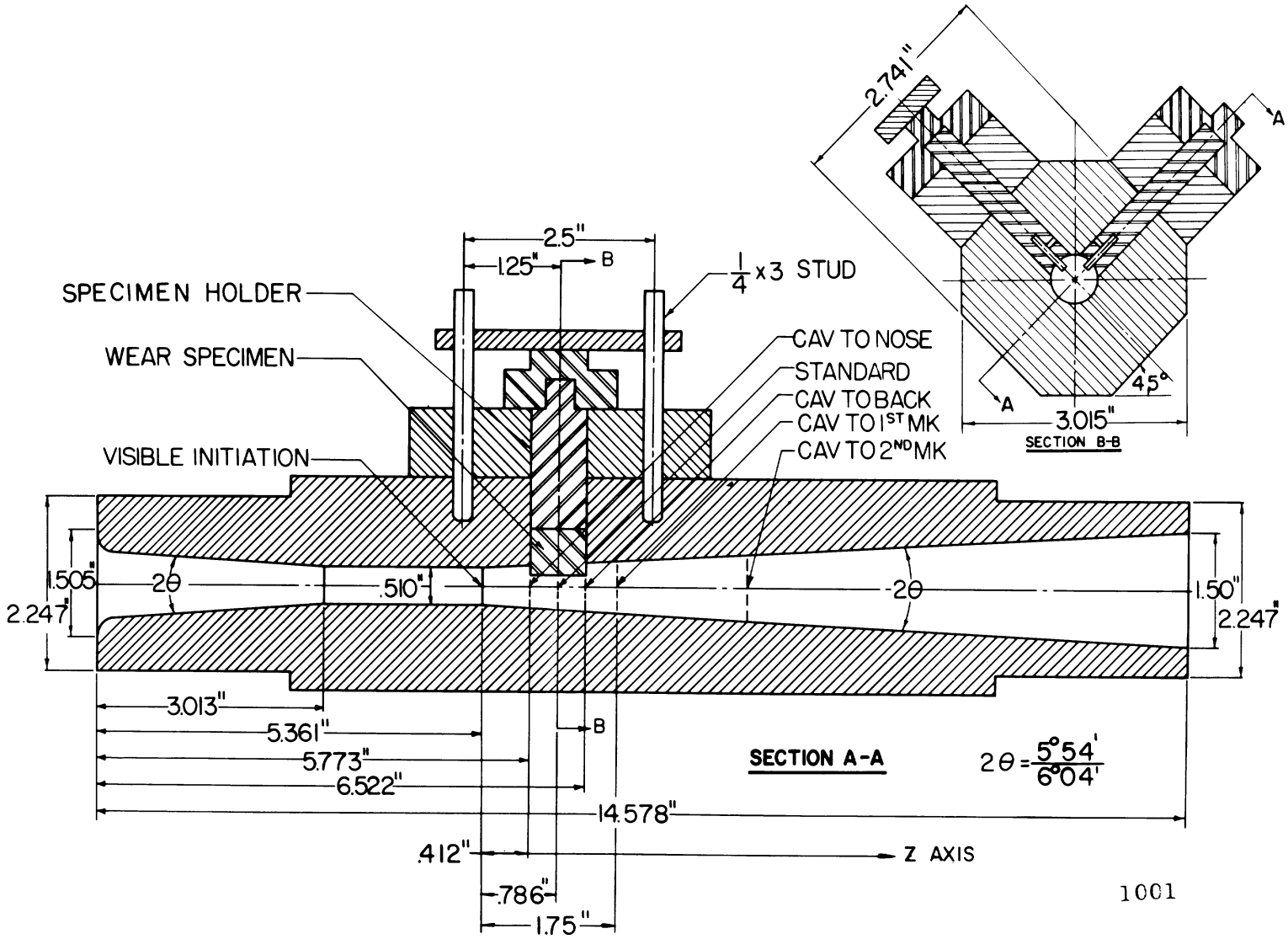

Figure 2 Cavitation Venturi Test Section.

To allow the accurate calculation of tensile properties from standard tensile tests and to assure maximum reproducibility of specimens, a non-streamlined, rectangular-shaped specimen was chosen. The specimen thickness was made as small as possible, consistent with the requirement that the percent differential in thickness between specimens not be excessive, to:

i) prevent excessive blockage of the channel

ii) minimize the cavitation induced by the specimen

iii) keep the applied force within reasonable limits

Hence a design thickness of 0.025" was selected. The axial specimen length was chosen to be the same as that of the standard unstressed specimens, i.e., 0.74".

A tension specimen is shown in Figures 3 and 4. The end thickness is sufficient[5] to assure that failure under a tensile test will occur in the mid-portion, which is exposed to the cavitating stream, before the end sections yield. The specimens are of annealed, 302-stainless steel blanks cut from 1/8" sheet stock. The mid-section is machined out by an end mill. No other finishing operation was performed on this section.

The specimen holders were made in two sections (Figures 5 and 6), and assembled as shown in Figures 7 and 8. The face of the oblong inner holder-section was machined to match that portion of the venturi removed to allow the insertion of the test specimen assembly. The circular holder extension was required for sealing, and to transmit the external load from the clamp.

The venturi used (Figure 9) had the same flow-path dimensions as that used with the conventional unstressed specimens,

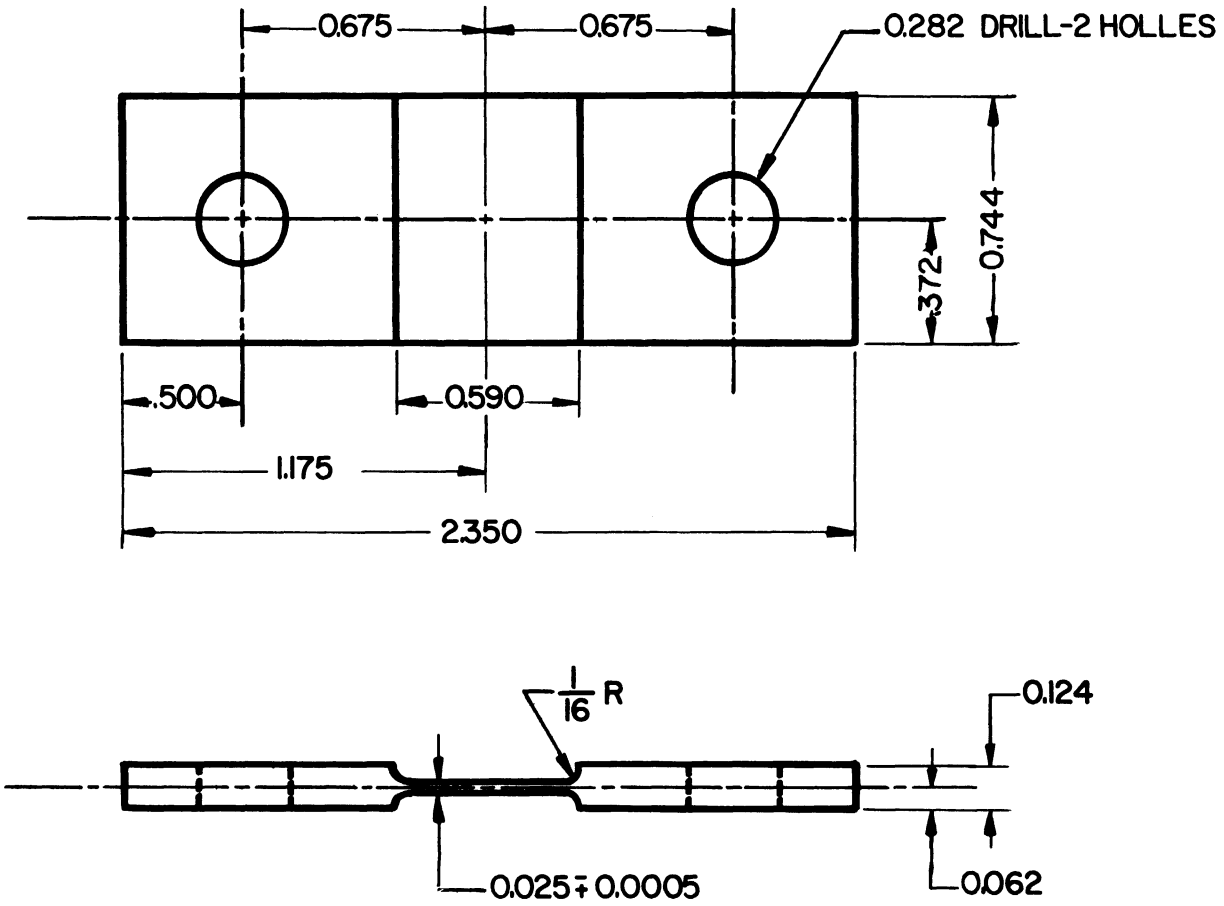

Figure 3 Drawing of Tension Test Specimen.

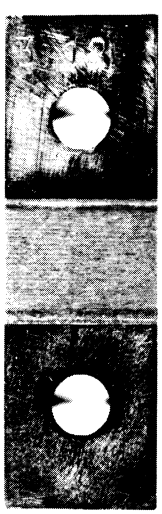

1287

1288

(a) Front View (b) Side View

Figure 4 Macrograph of Tension Test Specimen.

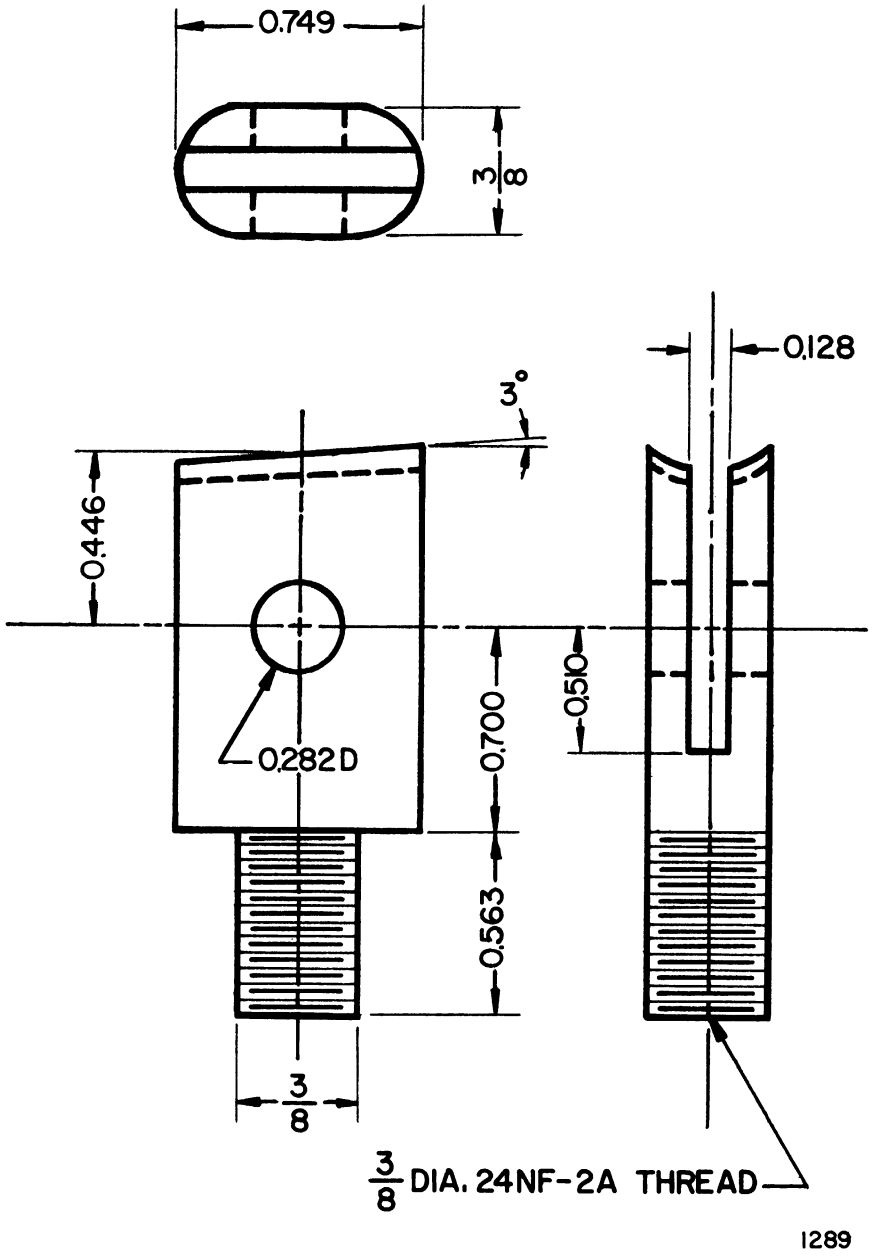

Figure 5 Drawing of Specimen Holder.

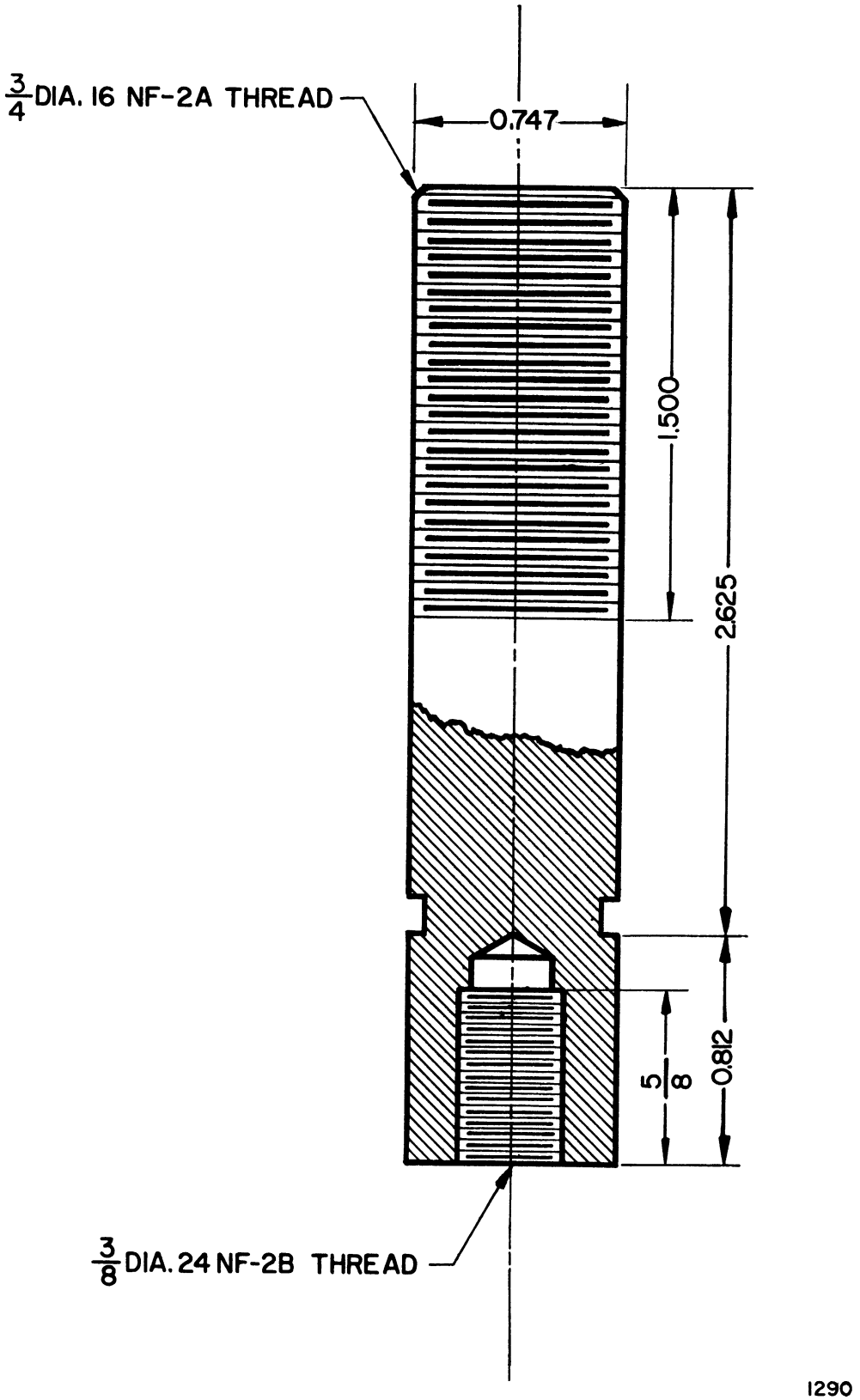

Figure 6 Drawing of Holder Extension.

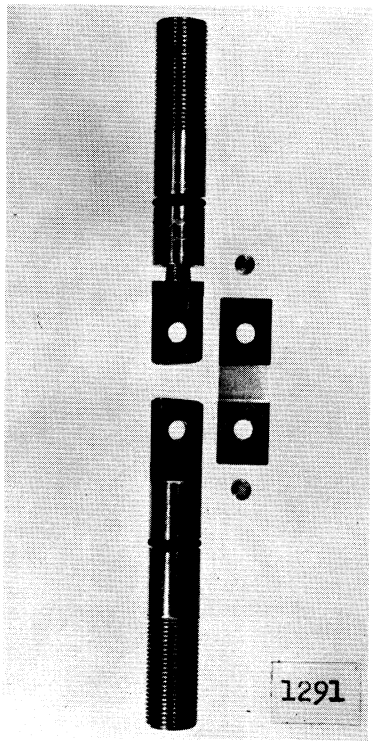

Figure 7 Macrograph of Holder Assembly.

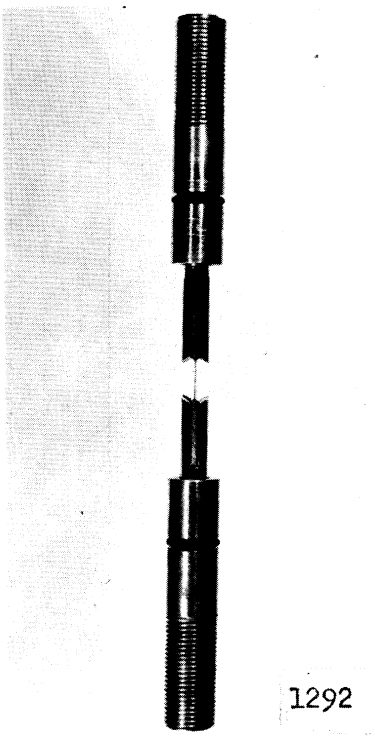

Figure 8 Macrograph of Holder Assembly.

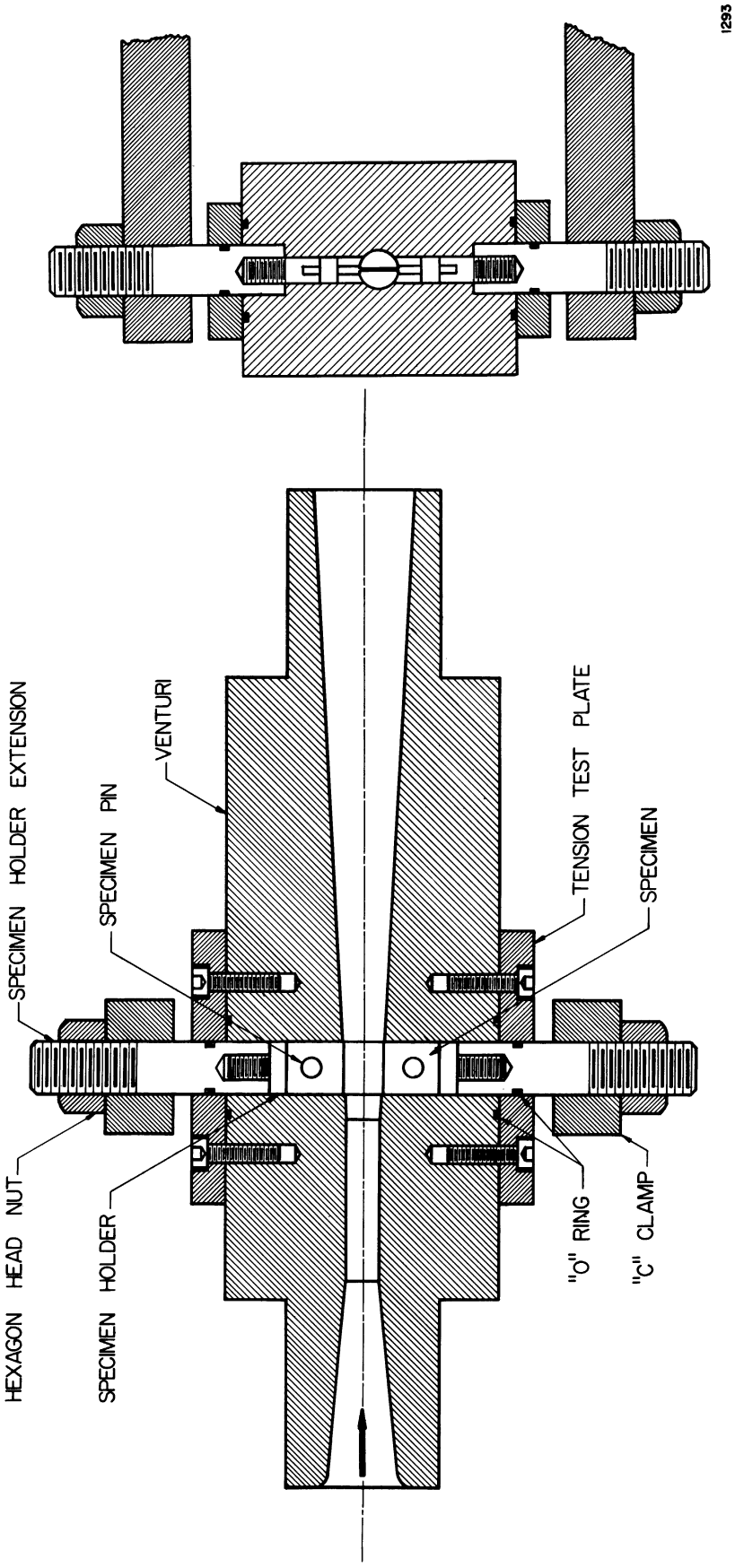

Figure 9 Assembly Drawing of Tension Test Venturi.

(Figure 2). The ports through which the test specimen assembly is inserted were sealed by two pairs of "O" rings:

i) between the plexiglas and the small steel plates on either side which are fastened to the venturi, and

ii) between the circular holder extension and the same plate.

The circular holders extend through holes in the ends of a heavy steel U-clamp which fits around the venturi (Figure 10). The external tensile load is applied to the specimen by tightening the large nuts on the threaded portion of the circular holder against the face of the clamp. Clamp load is measured by strain gages mounted on two of its vertical faces. Calibration was achieved by compressing the clamp in a load test machine. The load applied to a specimen can be determined from the calibration curve (Figure 11), which relates the clamp deflection, generated by tightening the nuts on the holders against the clamp, to the tensile load on the specimen.

2.3 Experimental Procedure

The experimental program consisted of two phases, (i) cavitation tests, and (ii) mechanical property tests.

The cavitation portion included tests on four specimens, loaded respectively, in the cavitation facility, to the stresses listed in Table I. Each specimen was tested in increments of three 5 hour runs, and five 15 hour runs (90 hours total) in room temperature mercury with a throat velocity of 34 feet per second. After each duration increment, the specimens were removed from the facility and weighed for damage determination.

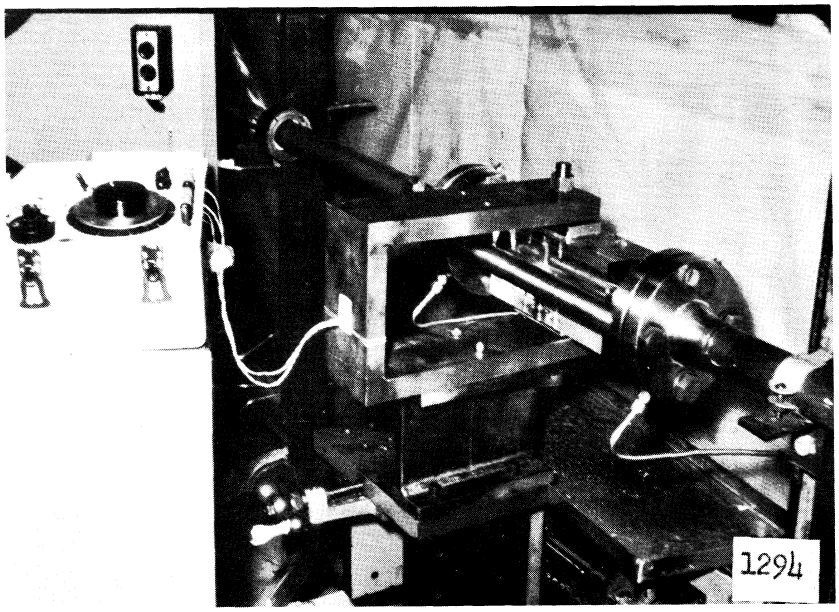

Figure 10 Photograph of Tension Clamp and Venturi.

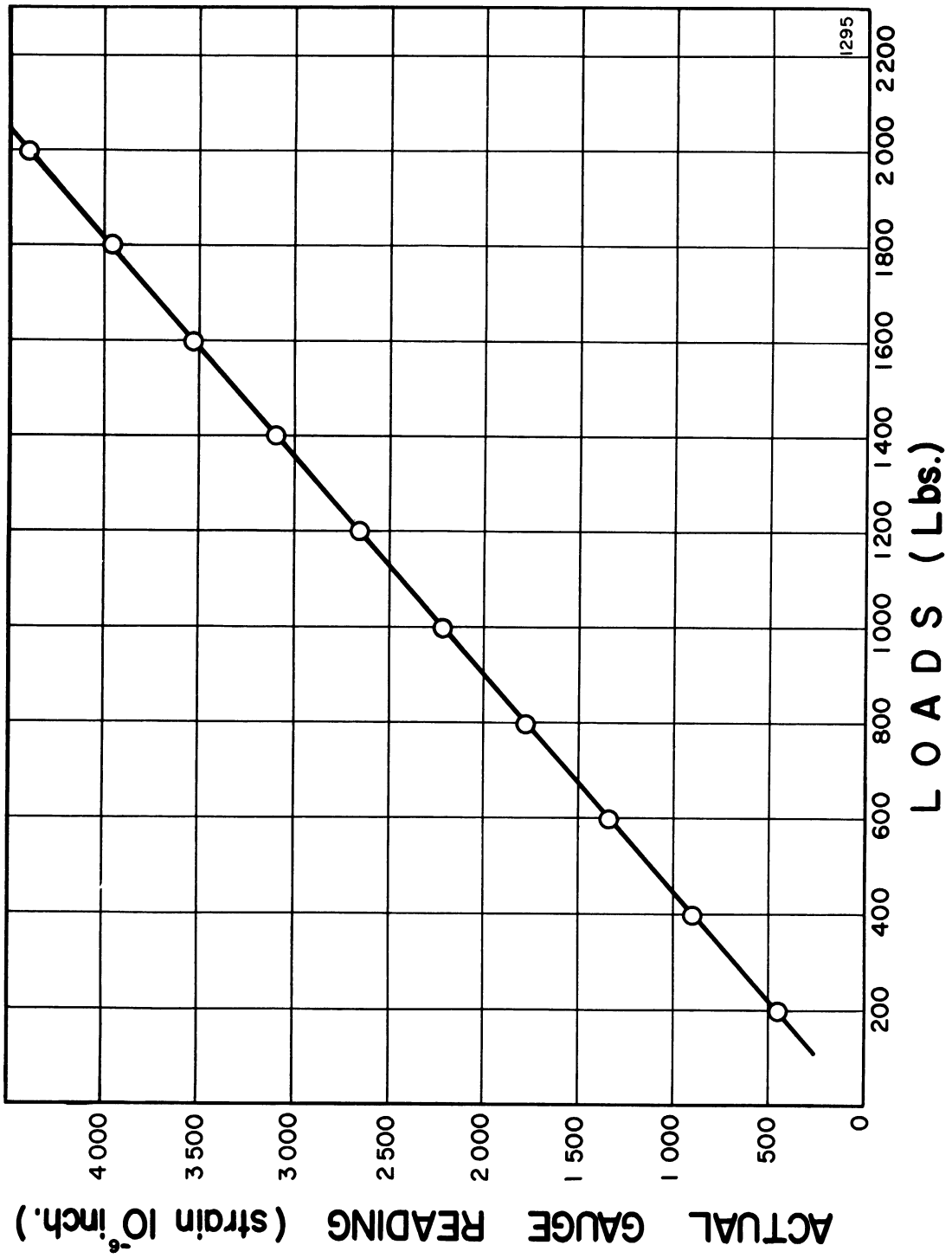

Figure 11 Tension Clamp Calibration Curve.

TABLE I

TENSILE LOADS FOR CAVITATION SPECIMENS

Specimen Number	Cross-Sectional Area (in^2)	Clamp Strain (10^{-6}in/in)	Tensile Load(lb)	Tensile Stress(psi)
3-7	0.01687	0	0	0
3-8	0.01603	830	375	23,400
3-5	0.01691	1765	794	46,900
3-18	0.01722	2625	1188	68,900

The cavitation termination, as visually determined, was at the axial midpoint of the specimen, i.e., analogous to "standard cavitation" as used with the conventional unstressed specimens (Figure 2).

Mechanical property tests, including yield and ultimate strength and hardness determinations, on both cavitated and uncavitated tension specimens were performed. Four uncavitated specimens and the four cavitated specimens were instrumented with strain gages (Figure 12) to determine their yield strengths and other details of their stress-strain curves, and were then broken to determine ultimate strength. Also, five other uncavitated specimens, but without strain gages, were broken to obtain additional tensile strength data. Hardness tests were made on specimens before and after breaking to determine their initial hardness as well as any change therein.

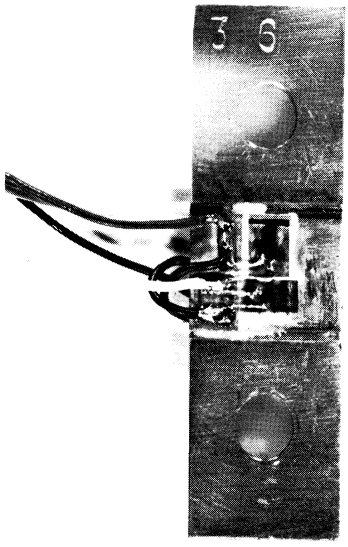

1296

Figure 12 Stainless Steel Specimen Number 6-3, Fitter With Strain Gages.

3.0 EXPERIMENTAL OBSERVATIONS

3.1 Mechanical Property Tests on Uncavitated Specimens

Nine uncavitated specimens were tested in a tensile machine to obtain their yield and ultimate strengths. The results are summarized in Table II, where values of yield strength appear only for those specimens with strain gages attached.

TABLE II

SUMMARY OF TENSILE TESTS ON UNCAVITATED SPECIMENS - ANNEALED STAINLESS STEEL TYPE 302

Specimen Number	Specimen Thickness	Yield Strength (psi)	Ultimate Strength (psi)
3-15	0.0235"	-	101,661
3-14	0.0202"	-	102,136
3-2	0.0240"	-	101,739
3-9	0.0242"	-	102,946
3-12	0.0187"	-	102,516
3-6	0.0225"	50,700	100,262
3-23	0.0222"	55,000	104,282
3-24	0.0225"	50,400	102,751
3-19	0.0174"	54,100	103,502

Average Yield Strength = 52,550 $^{+4.66\%}_{-4.09\%}$ (Standard Deviation = 3.97%)

Average Ultimate Strength = 102,422 $^{+1.81\%}_{-2.11\%}$

(Standard Deviation = 1.07%)

The average ultimate strength was found to be 102,422 psi ($\pm$ 2%, standard deviation = $\sim$ 1%). The yield strengths were determined by the 0.2% offset method. An average value of

52,550 psi ($\pm \sim 4.3\%$, standard deviation $\sim 4\%$) was obtained. The stress-strain curves for the four specimens instrumented with strain gages are shown in Figures 13-16. Figure 17 shows a typical specimen after fracture.

Hardness tests on three specimens resulted in an average hardness of about 85 Rockwell B, and showed no appreciable difference in hardness between the thin, milled portion, and the thicker sheet-stock portion of a specimen (see Figures 18 and 19). As expected, hardness tests on fractured specimens before and after breaking showed that the thin test section became much harder after being fractured, (Figures 20 and 21). Hardness tests on a specimen before and after loading to about half its yield strength (no plastic elongation could be detected) showed no appreciable change in hardness of either the thin test section or the thicker stock portion (Figure 22).

3.2 Quantitative Damage Results of Cavitation Tests

As previously mentioned in section 2.3, four specimens were tested, under four different tensile loads, respectively, each for 90 hours total (with weighing intervals as previously given) in the cavitating mercury at the same flow and cavitation condition. Weight loss in general increases with tensile load (Figure 23), 8% from zero to maximum load. This cannot be considered as definitely beyond possible scatter, but may well represent a trend which will be substantiated by further experimentation.

Figure 24 shows the same data in terms of mean depth of penetration (i.e., volume loss per unit area of the surface of a

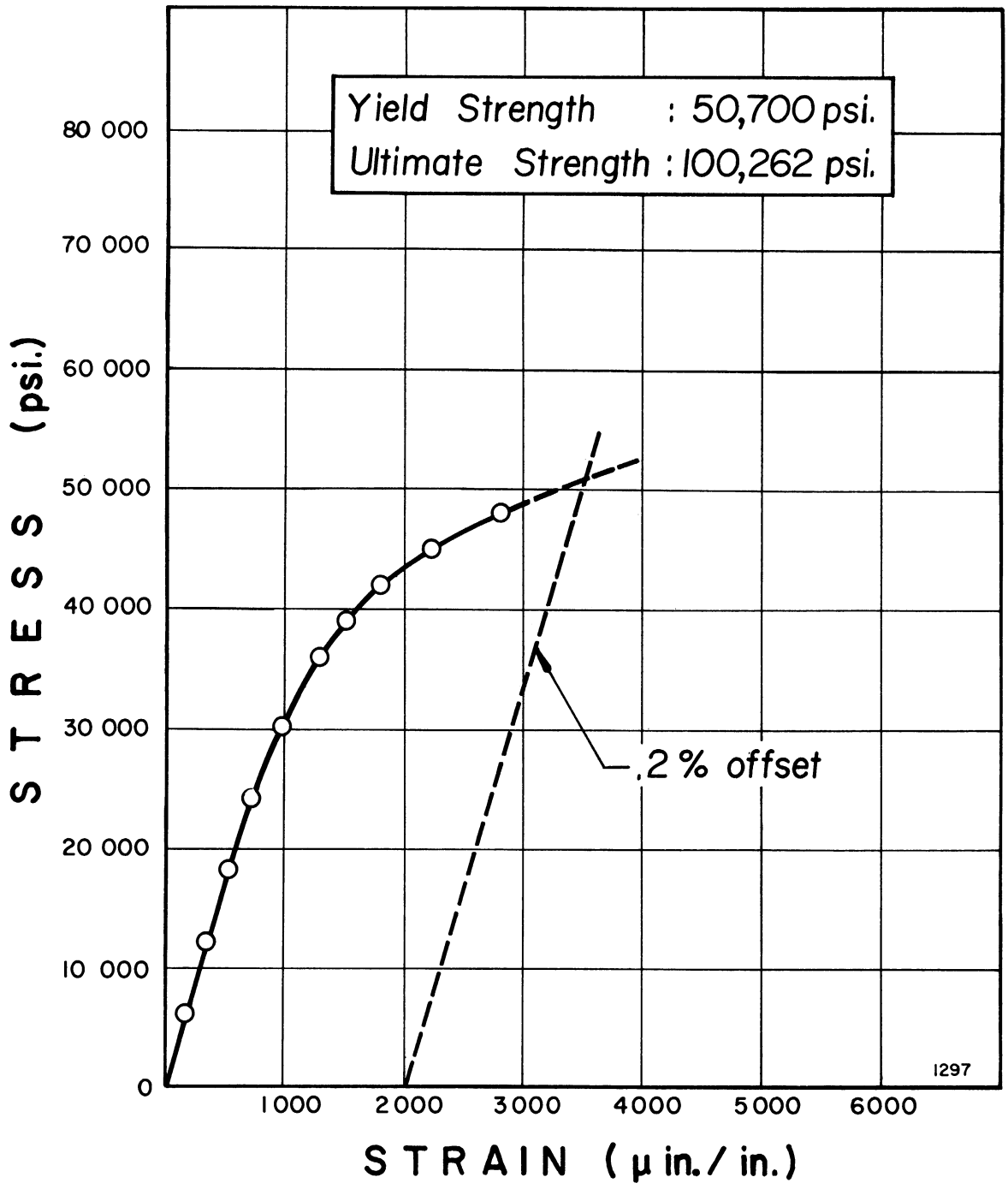

Figure 13 Stress-strain Diagram for Uncavitated Specimen #6.

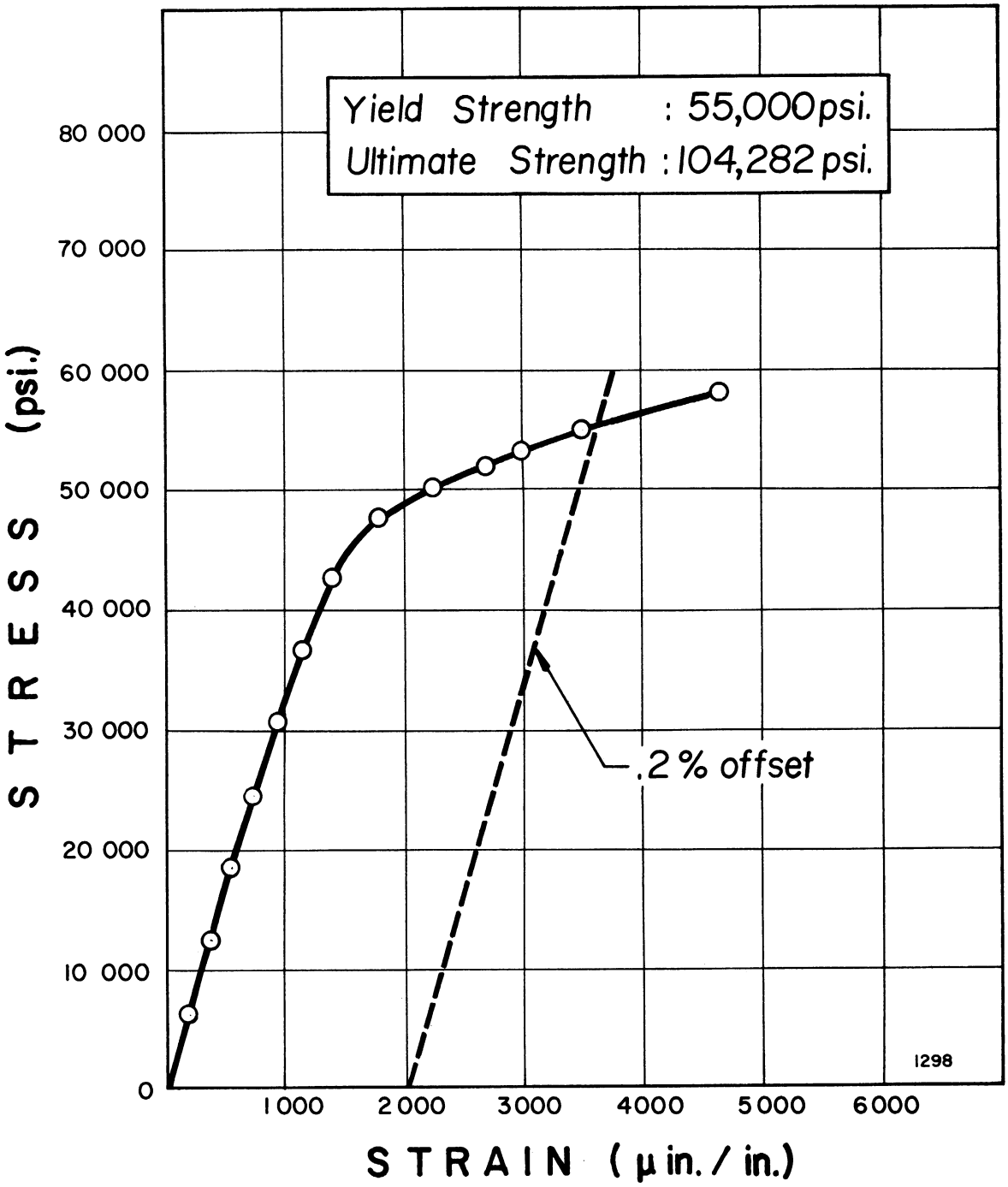

Figure 14 Stress-strain Diagram for Uncavitated Specimen #23.

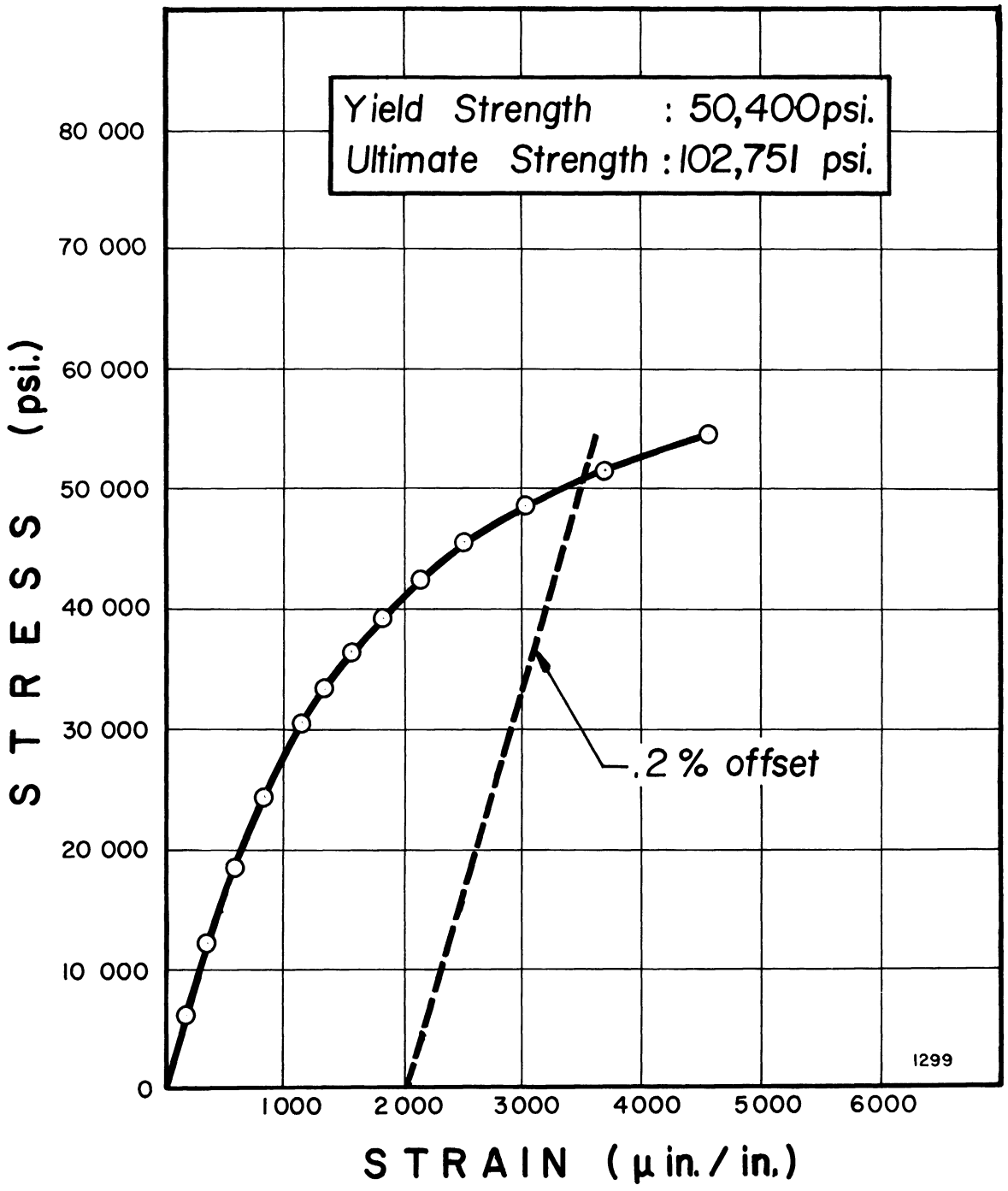

Figure 15 Stress-strain Diagram for Uncavitated Specimen #24.

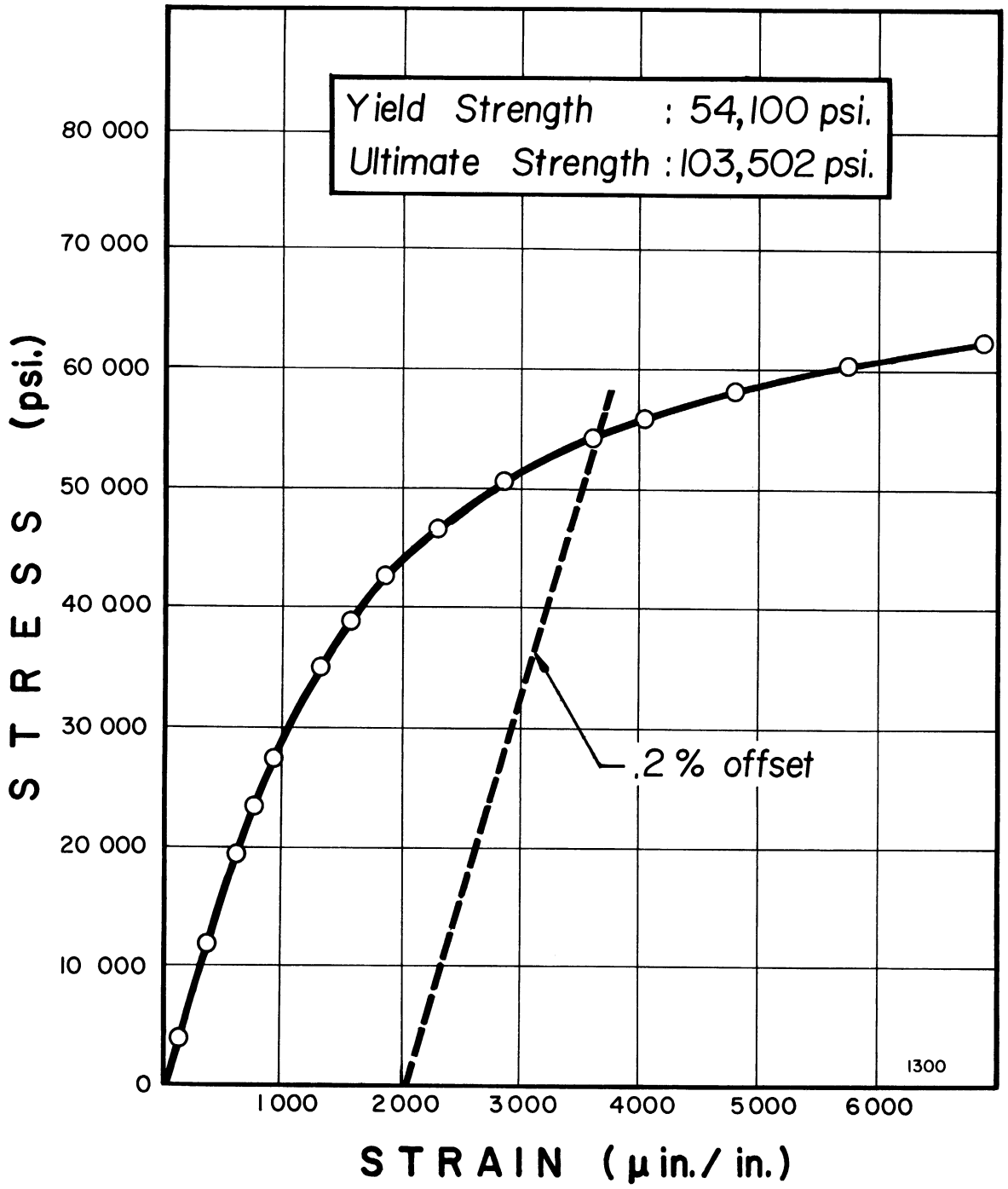

Figure 16 Stress-strain Diagram for Uncavitated Specimen #19.

1301

Figure 17 Stainless Steel Specimen Number 2-3, After Fracture in Tensile Test.

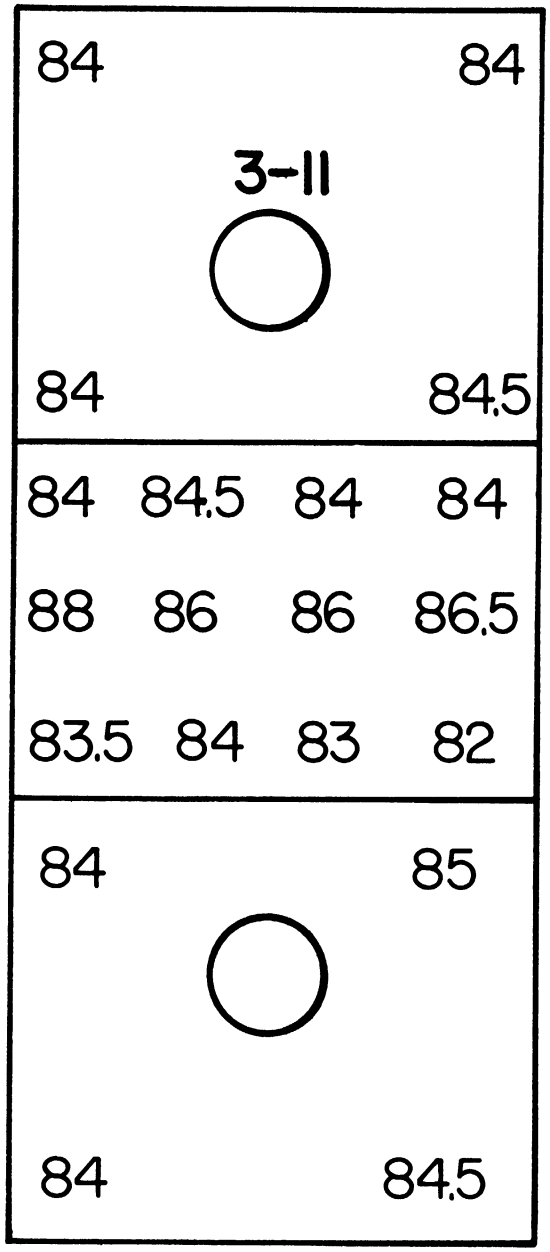

1302

Figure 18 Drawing of Uncavitated Hardness Test Specimen #11.

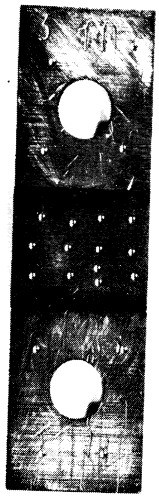

1303

Figure 19 Stainless Steel Specimen Number 11-3, Showing Locations of Hardness Readings.

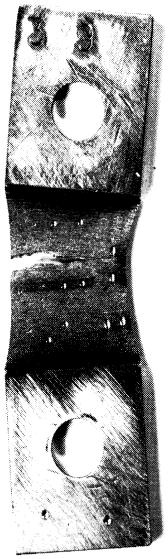

1304

Figure 20 Stainless Steel Specimen Number 9-3, After Fracture in Tensile Test, Showing Locations of Hardness Readings.

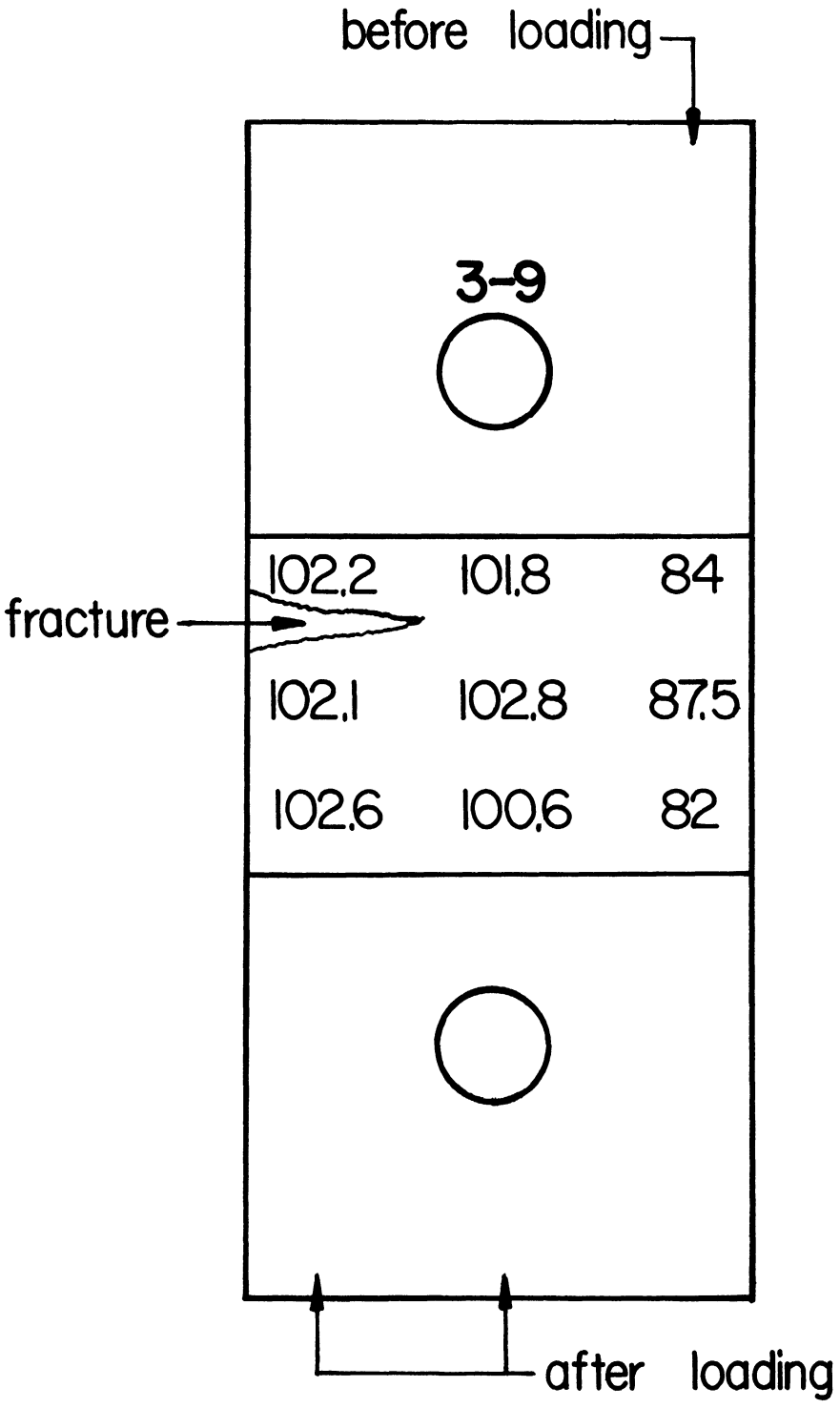

Figure 21 Drawing of Fractured Hardness Test Specimen #9.

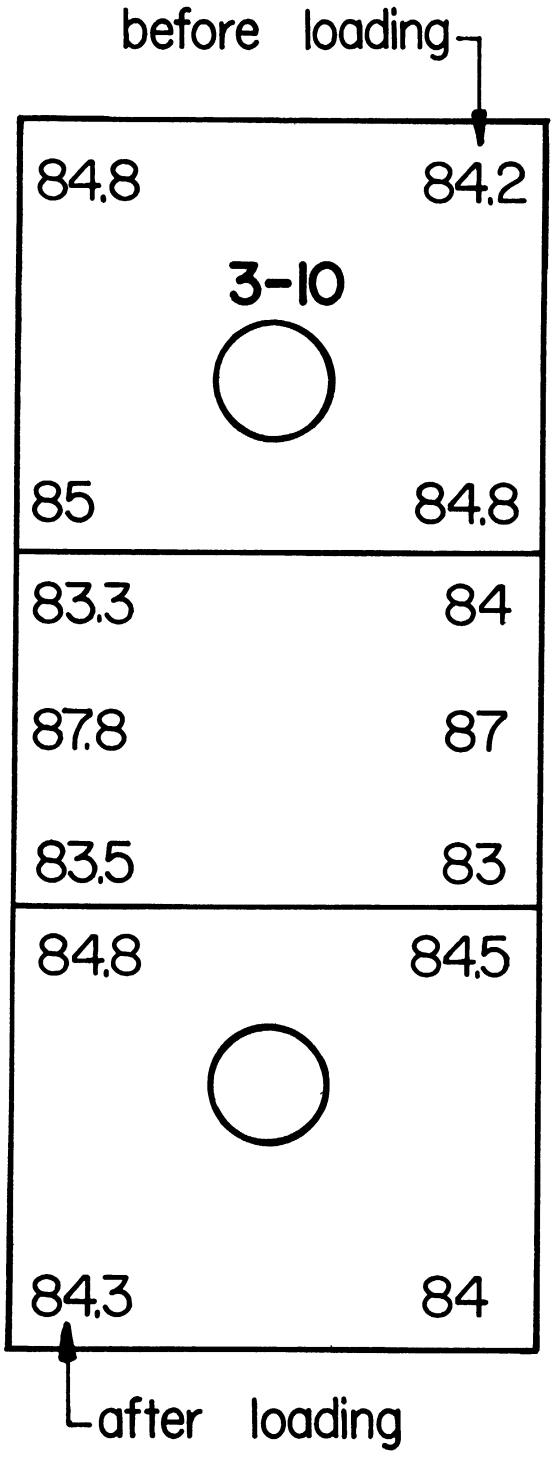

Figure 22 Drawing of Hardness Specimen Loaded to 30,270 psi.

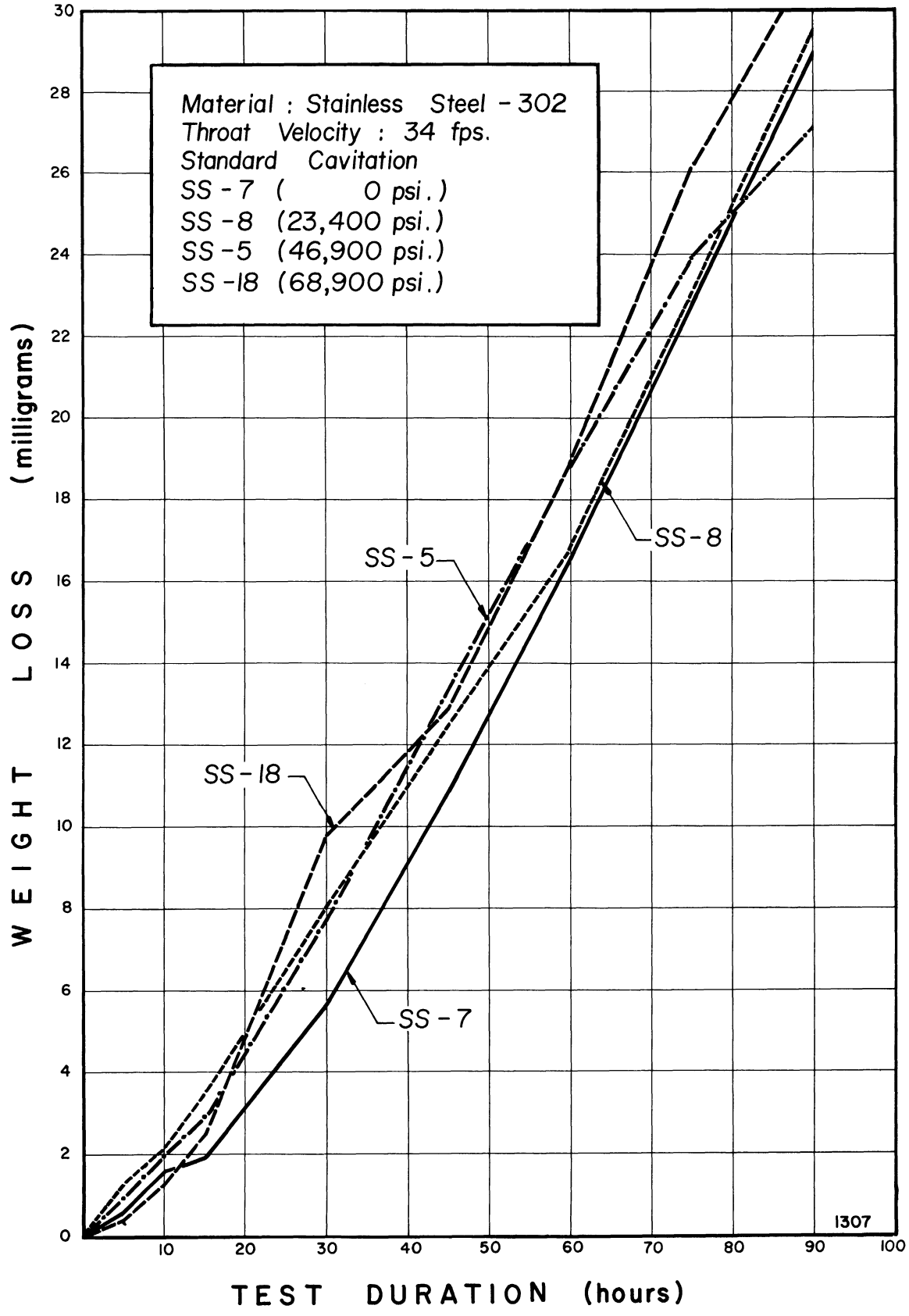

Figure 23 Weight Loss vs Test Duration for Cavitation Damage Specimens.

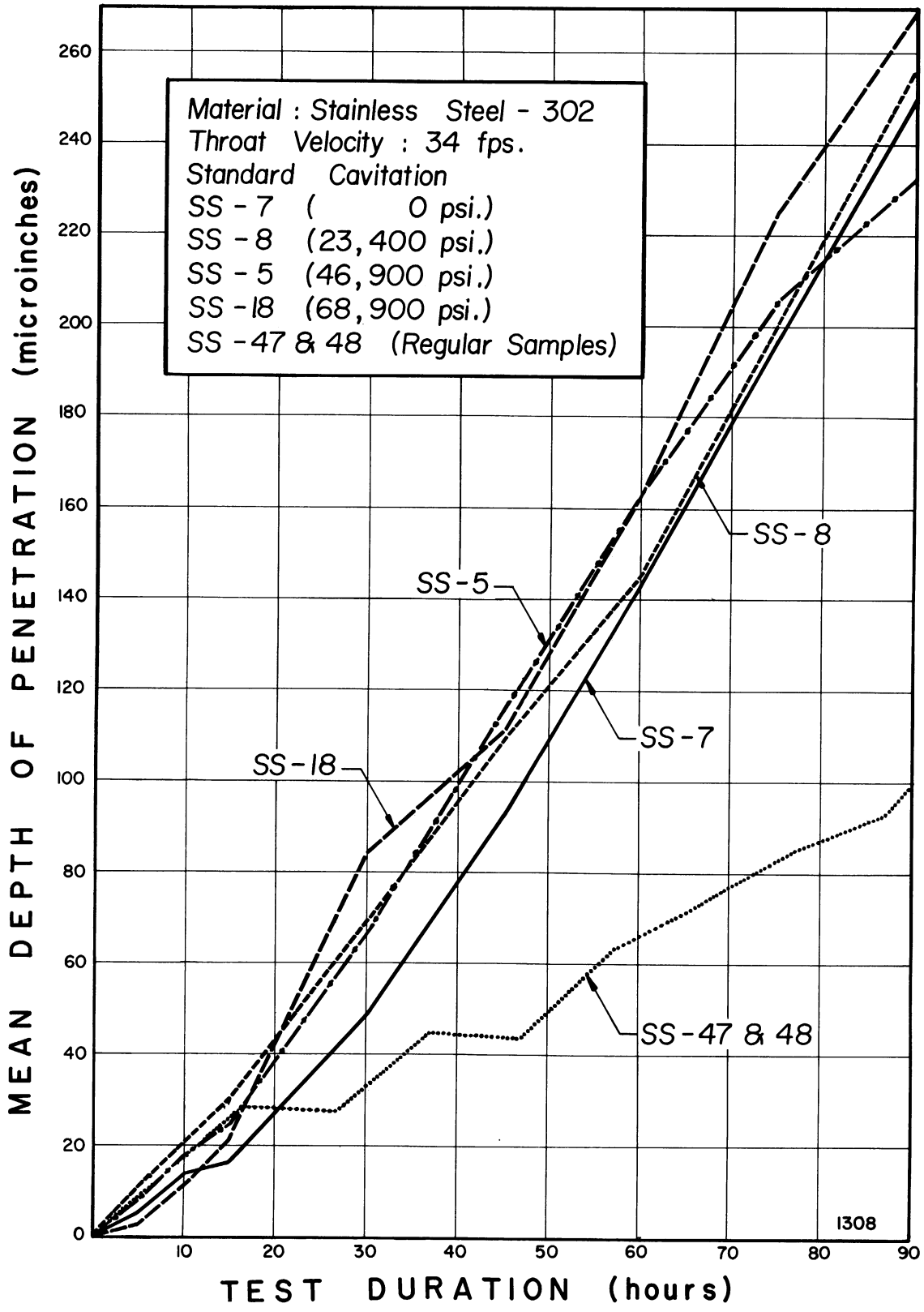

Figure 24 Mean Depth of Penetration vs. Test Duration for Cavitation Damage Specimens.

specimen exposed to cavitation) as a function of duration. For comparison, the mean depth of penetration of two conventional (unstressed) specimens, tested together at the same velocity and cavitation condition as the tensile specimens, is included. Due presumably to their non-streamlined shape, and the resultant high level of self-induced cavitation, the tensile specimens received more than twice the mean depth of penetration as the conventional specimens in 90 hours.

The majority of the pitting is confined to the downstream half of each specimen (Figures 25-28), slightly downstream of the visual termination of cavitation. This is consistent with the general pattern of pitting observed in the tests with conventional specimens. The maximum size of the pits incurred is about 2 to 3 mils.

3.3 Mechanical Property Tests on Cavitated Specimens

All four specimens tested in the cavitation facility were instrumented with strain gages and broken in a tensile test machine to determine their yield and ultimate strengths. The results are summarized in Table III.

1309

(a)

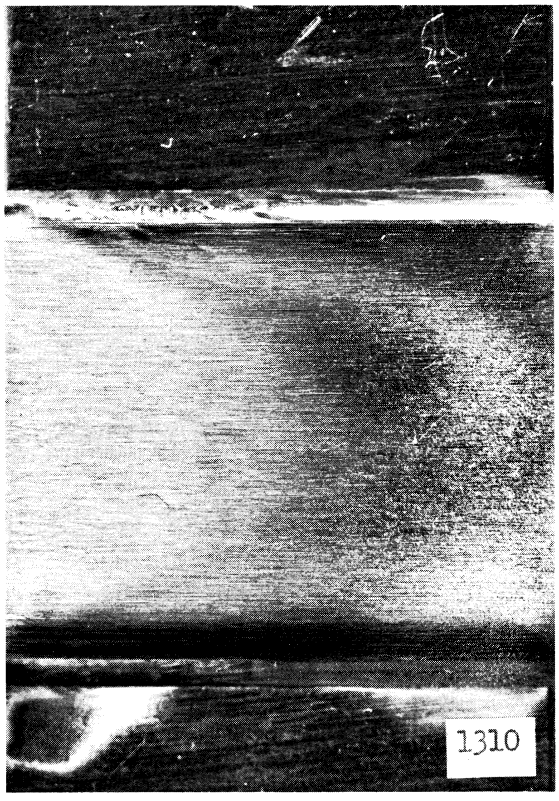

(b)

Figure 25 (a) Stainless Steel Specimen Number 7-3, After Cavitation, (b) Blow-up of Center Portion of (a).

1311

(a)

(b)

Figure 26 (a) Stainless Steel Specimen Number 8-3, After Cavitation, (b) Blow-up of Center Portion of (a).

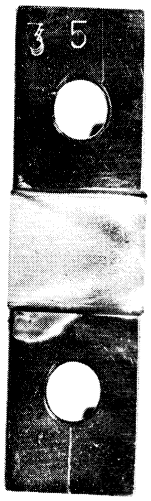

1313

(a)

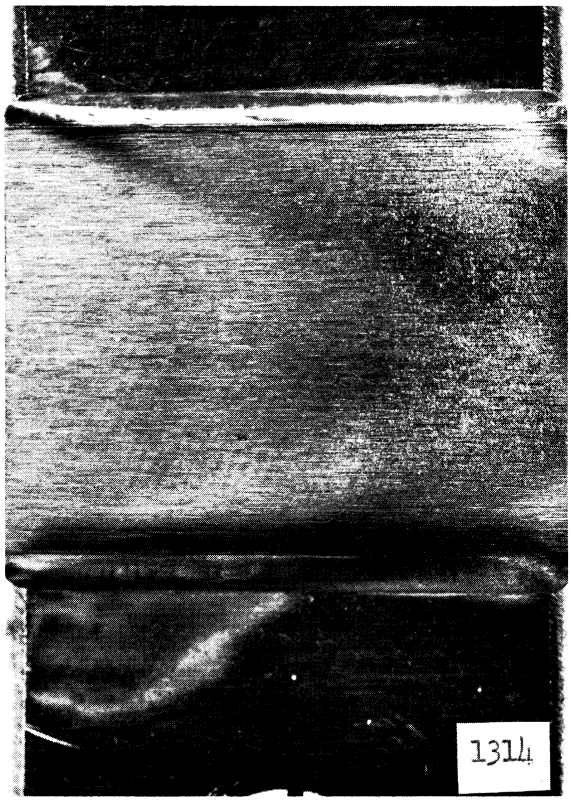

(b)

Figure 27 (a) Stainless Steel Specimen Number 5-3, After Cavitation, (b) Blow-up of Center Portion of (a).

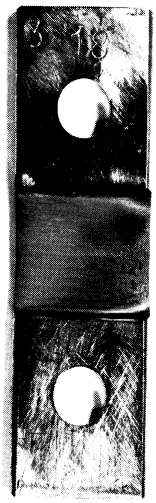

1315

(a)

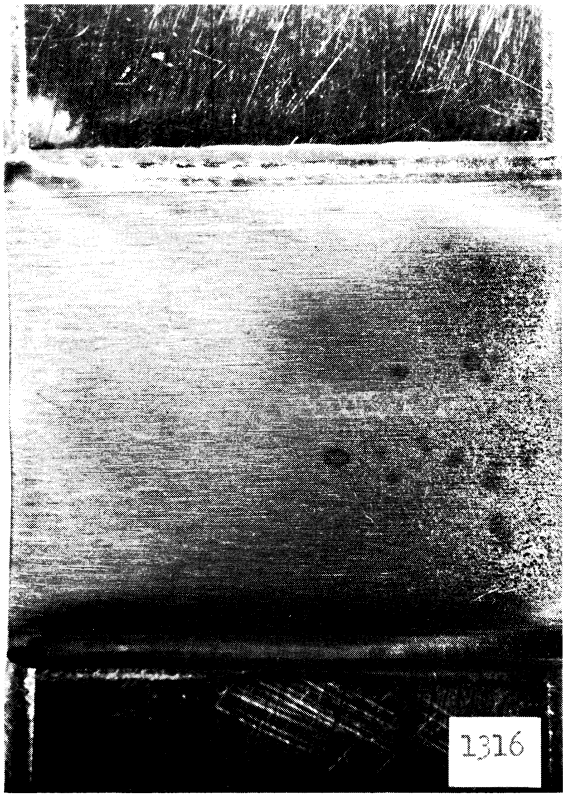

(b)

Figure 28 (a) Stainless Steel Specimen Number 18-3, After Cavitation, (b) Blow-up of Center Portion of (a).

TABLE III

SUMMARY OF TENSILE TESTS ON CAVITATED SPECIMENS --

ANNEALED STAINLESS STEEL TYPE 302

Specimen Number	Specimen Thickness	Test Load(psi)	Yield Strength (psi)	Ultimate Strength (psi)
3-7	0.0227"	0	47,700	94,761
3-8	0.0217"	23,400	44,800	93,101
3-5	0.0227"	46,900	54,100	92,787
3-18	0.0232"	68,900	67,200	90,055
Uncavitated Average	----	----	52,550	102,422

Comparing the yield and ultimate strengths (Table III) with the average values determined for new specimens (Table II, repeated in Table III for convenience), the ultimate strength of the cavitated specimens decreases monatomically from about 7½% to 12%, from the average value for the uncavitated specimens, as test load increased, although the variation in mean "undamaged thickness" is much less (about 2% maximum, as discussed later). Yield strength similarly decreased considerably for those specimens with loads well below the yield strength. These data are all listed in Table IV and plotted in Figure 39.

TABLE IV

DECREASE IN MECHANICAL STRENGTH PROPERTIES

OF CAVITATION DAMAGED SPECIMENS

Specimen Number	Test Load	MDP(u") (90hrs)	YS (psi)	%Decrease YS	US (psi)	%Decrease US
3-7	0 psi	250	47,700	9.23	94,761	7.48
3-8	23,400	255	44,800	14.74	93,101	9.10
3-5	46,900	233	54,100	-2.95*	92,787	9.40
3-18	68,900	270	67,200	-27.9*	90,055	12.08

* Minus sign denotes increase in yield strength.

The stress-strain diagrams used to obtain the yield strength of the four damaged specimens are shown in Figures 29-32. Hardness checks prior to breaking indicated no appreciable difference between the hardness of the cavitation-damaged specimens and the uncavitated specimens.

In the tensile test machine, all the cavitated specimens failed first at the downstream edge, i.e., region of heavy cavitation damage, (Figure 33, e.g.), whereas the uncavitated specimens failed at random regions at either end of the specimens (Figure 17, e.g.).

3.4 Specimen Micrometallurgical Examinations

Photomicrographs of etched cross-sections through damaged and non-damaged regions of specimens have been made in an attempt to determine how far the damage has penetrated, and how substantial an effect on the gross strength properties of

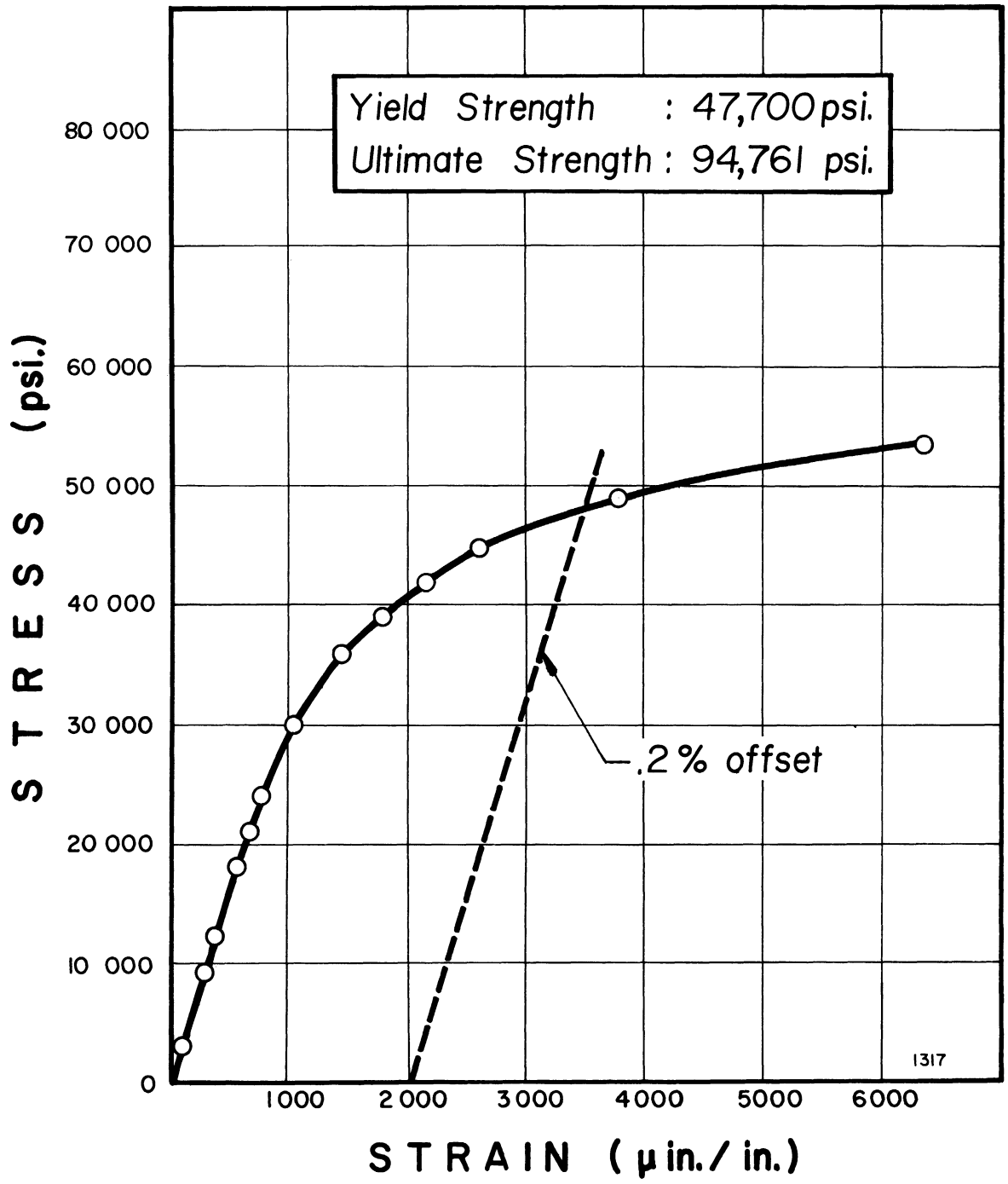

Figure 29 Stress-strain Diagram for Damage Specimen #7.

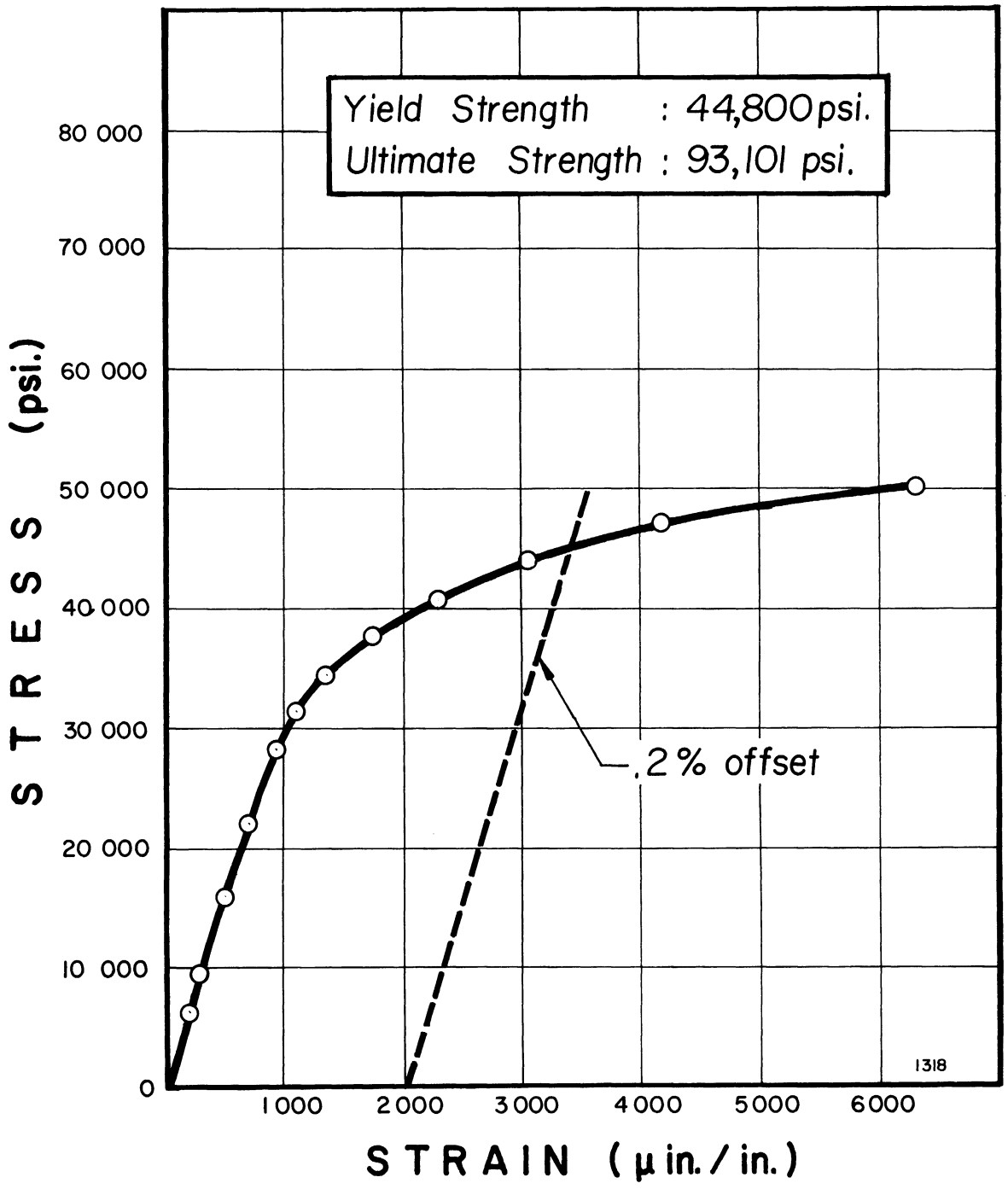

Figure 30 Stress-strain Diagram for Damage Specimen #8.

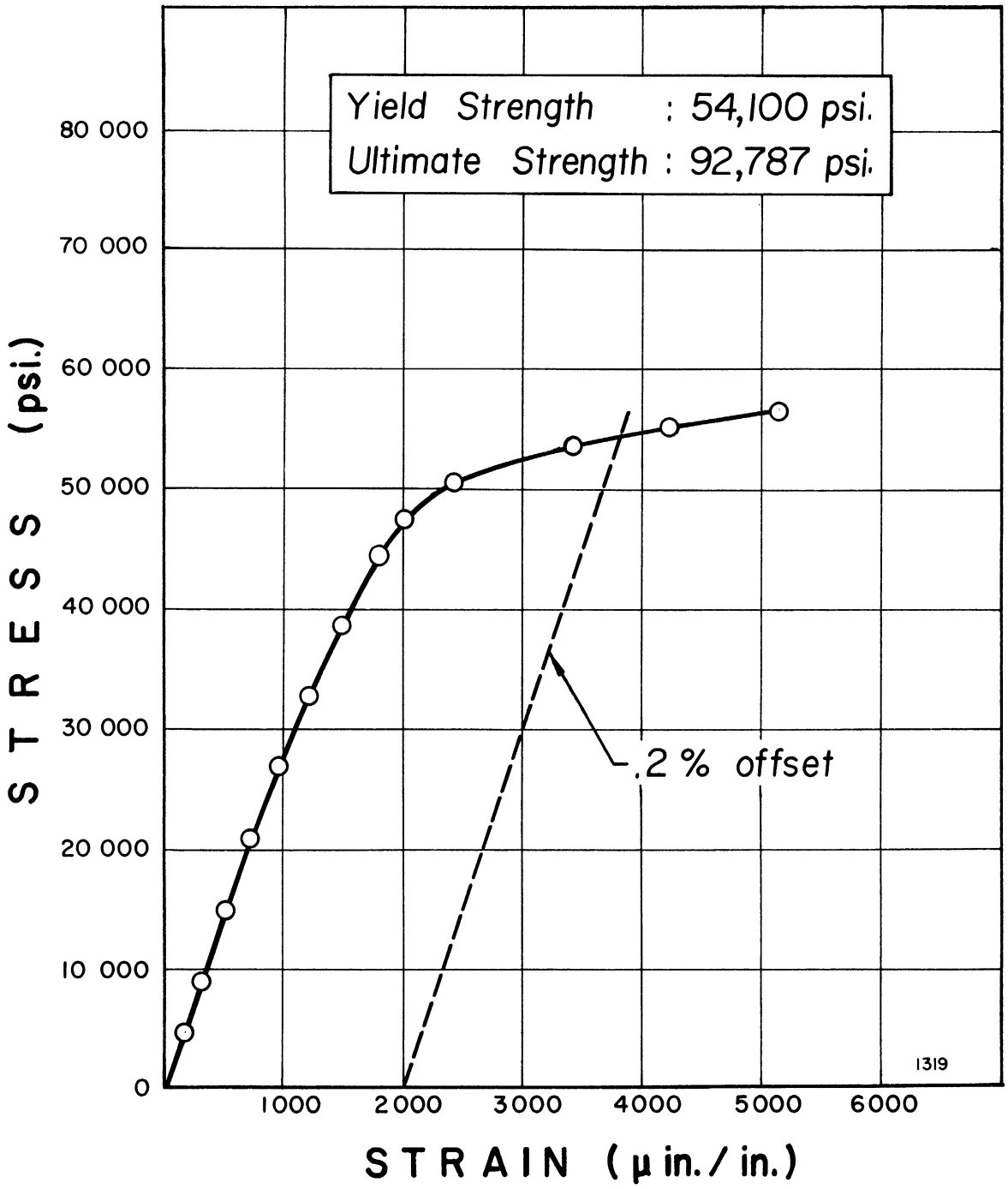

Figure 31 Stress-strain Diagram for Damage Specimen #5.

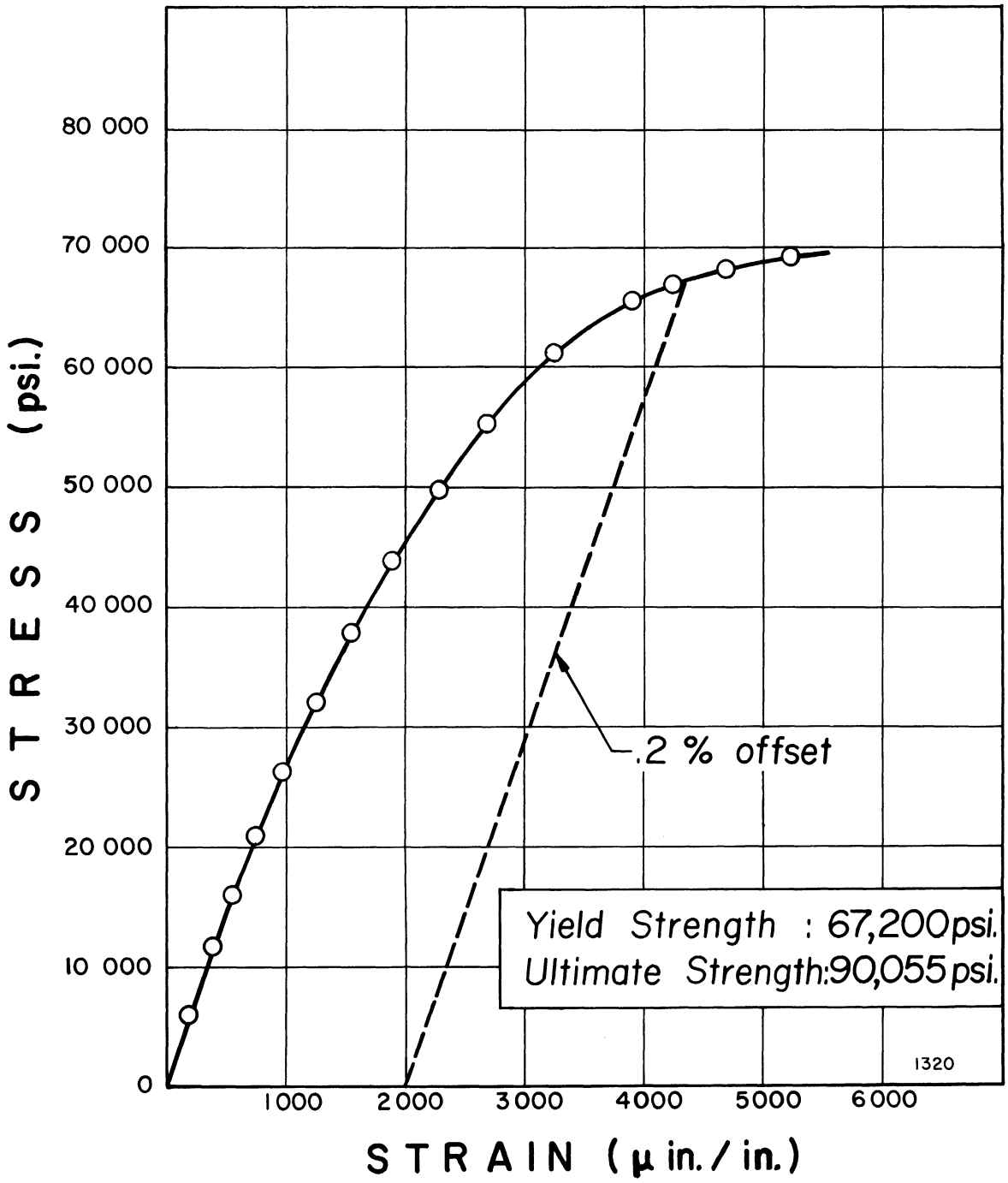

Figure 32 Stress-strain Diagram for Damage Specimen #18.

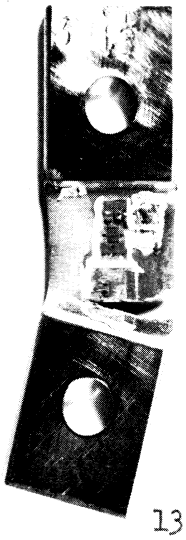

1321

Figure 33 Stainless Steel Specimen Number 18-3, After Cavitation Damage and After Fracture in Tensile Test, Showing Marks Where Strain Gages Were Attached.

the specimens might be expected. In particular it was thought that microcracks, generated by the cavitation, might penetrate relatively deeply.

Figure 34- a and b shows a typical cross-section from an uncavitated specimen, at 100X and 1000X, respectively. Figure 35- a and b is a similar typical section through a region of relatively light cavitation damage, and Figures 36 - a and b and 37-a through a region of relatively heavy damage. Figure 37-b is a cross-section through a heavily cavitated region from the centrifugal pump impeller of the mercury loop (SS-type 316), included for comparison. Examination of these photomicrographs shows that the surface irregularities in the uncavitated surface have a depth of about 0.1 mils, in the region of lighter cavitation damage about 0.35 mils, and in the region of heavier damage, both from the tensile specimen and the pump impeller, 1.5 to 3 mils. The examination has not disclosed any evidence of substantial penetration of microcracks, etc., below the level of rather gross damage shown in these photos. However, as will be shown later, the local depth of pitting herein observed (although not the mean depth of penetration) is of the order of magnitude necessary to explain the measured reduction in tensile and yield strength of the cavitated specimens.

4.0 DISCUSSION OF EXPERIMENTAL RESULTS

4.1 Effect of Applied Tensile Stress on Weight Loss

As previously mentioned, there was a slight but relatively consistent, increase of weight loss with applied

(a)

(b)

Figure 34 Photomicrograph of Cross-Section of Uncavitated Specimen (a) 100X, (b) 1000X.

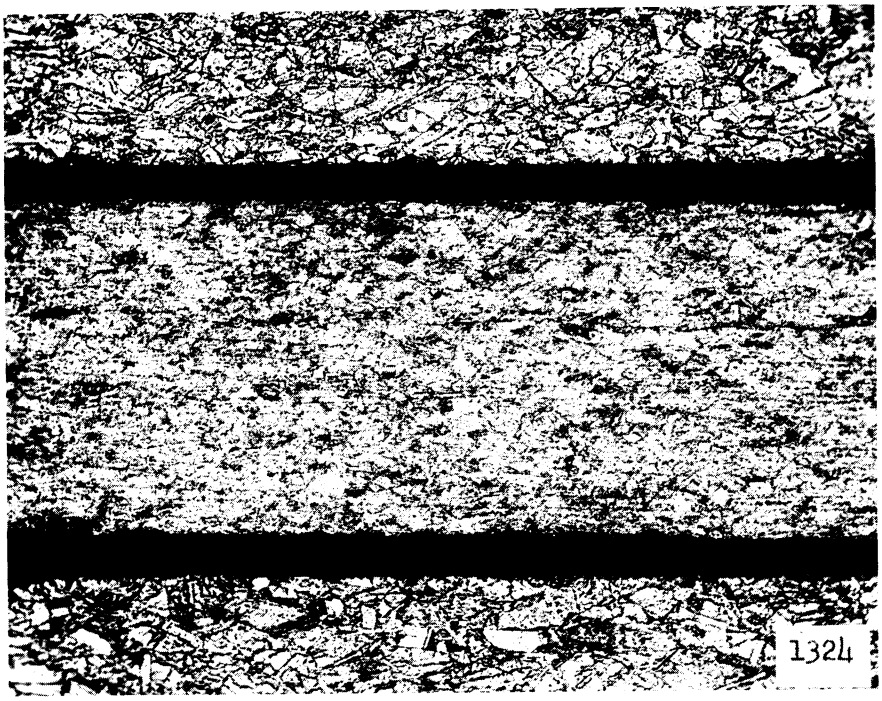

(a)

(b)

Figure 35 Photomicrograph of Cross-Section of Lightly Cavitated Specimen (a) 100X, (b) 1000X.

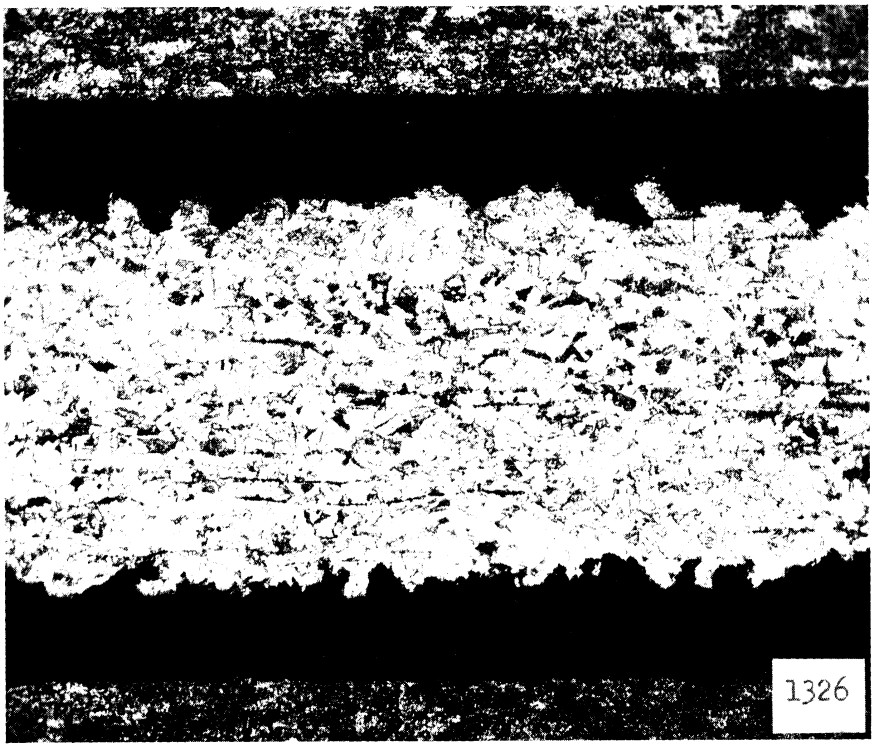

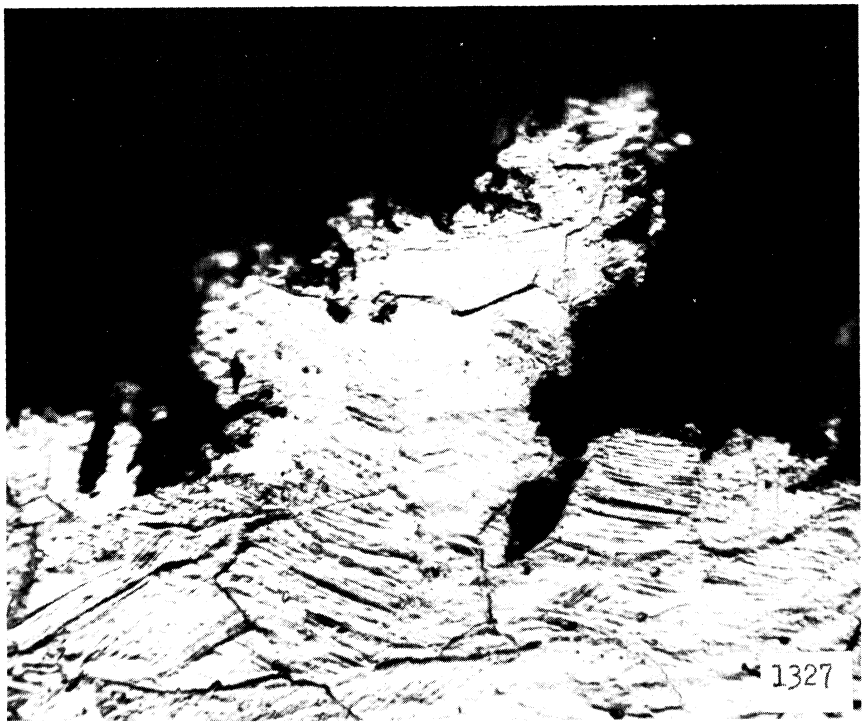

(b)

Figure 36 Photomicrograph of Cross-Section of Heavily Cavitated Specimen.

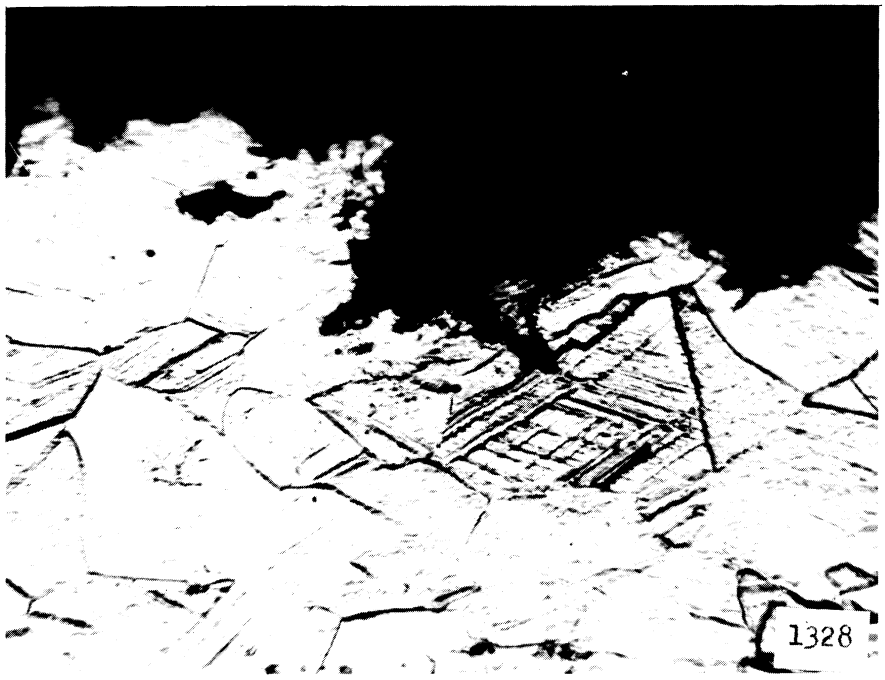

(a)

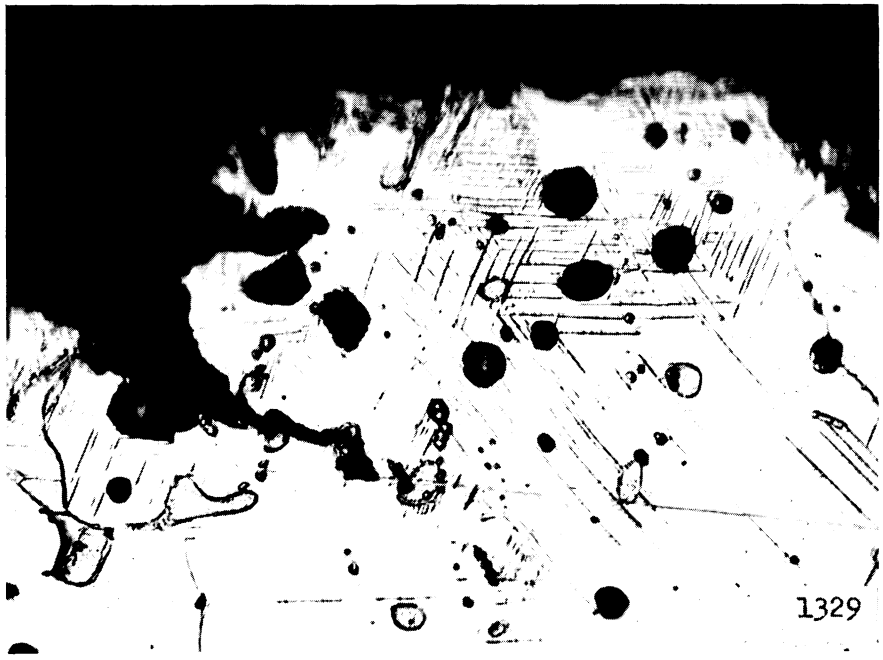

(b)

Figure 37 (a) Photomicrograph of Cross-Section of Heavily Cavitated Specimen at 100X. (b) Photomicrograph of Cross-Section of Heavily Cavitated Region of 316 SS Centrifugal Pump Impeller at 1000X.

tensile load. At least two possible mechanisms exist.

4.1.1 Alteration of Local Loading From Applied Load

The application of a substantial external load, acting with the local stresses caused by bubble implosions (or other hypothesised cavitation-damage mechanisms), will certainly alter the stress pattern from that due purely to cavitation. Figure 38 is a diagram of a typical portion of the surface of one of the tensile specimens under cavitation attack. Assuming as a first approximation the maximum shear stress failure model, the failure criterion becomes the maximum absolute magnitude of the difference between principal stresses. As can be seen from the diagram of Figure 38, the likelihood of failure under cavitation attack is increased by applied uniaxial tensile load, if the failure occurs in that portion of the region around the impingement of shock waves from cavitation bubble implosions which is subjected to compressive loading by the cavitation. The likelihood of failure is decreased if it is to occur in a region subjected to tensile loading by the bubble implosions.

4.1.2 Formation of Microcracks

It might be expected that the propagation of microcracks would be more extensive under the condition of an applied tensile load. Crack formation is consistent with the hypothesis that much of the material removal in cavitation damage is due to fatigue failure. However, as already mentioned, the examination of sections from the cavitated regions has not as yet substantiated this theory.

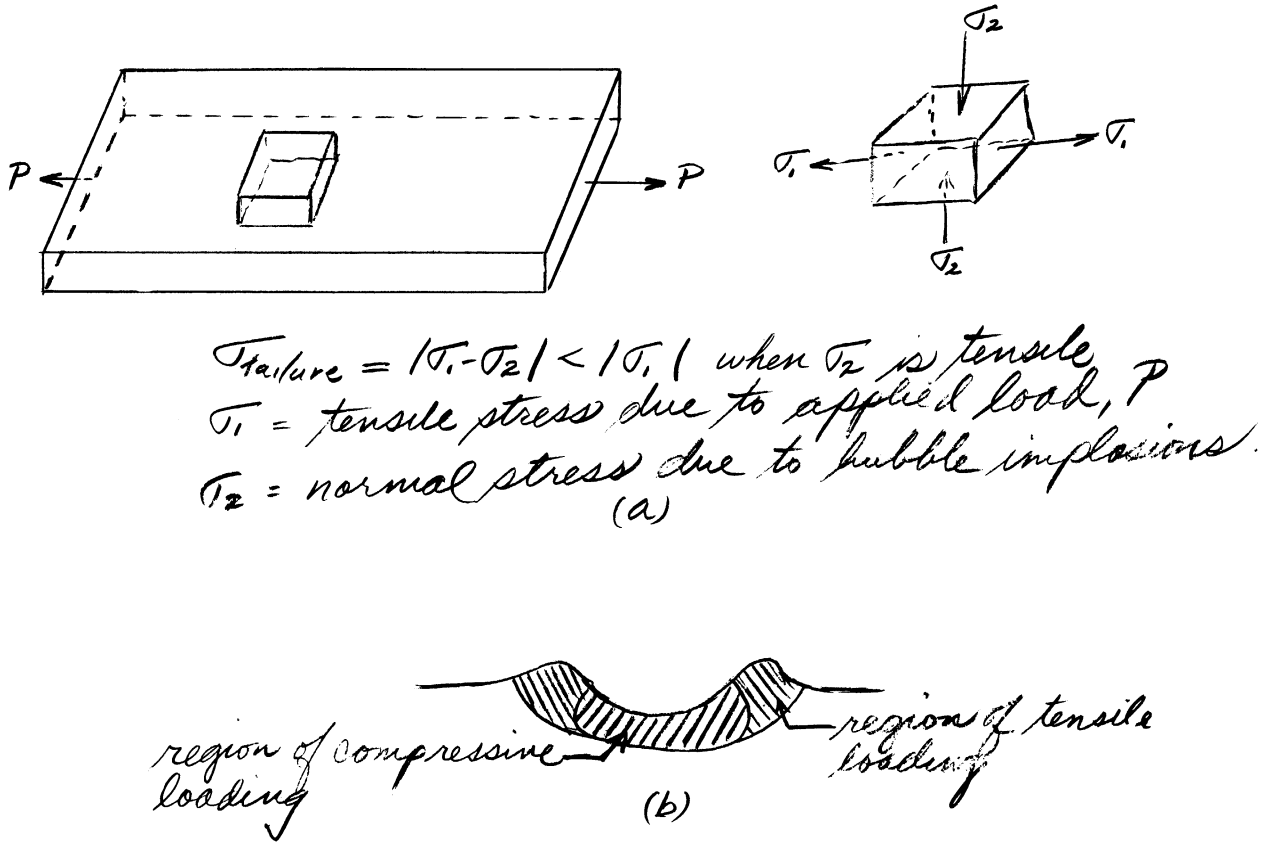

Figure 38 (a) Schematic Diagram of Typical Section From Tensile Specimen Depicting Stresses. (b) Sketch of Typical Cavitation Pit.

4.2 Effect of Damage and Applied Stress on Strength Properties

The present tests provide, to the authors' knowledge, the first published measurement of the effect of a known quantity of cavitation damage on the gross mechanical properties of test specimens. Also, for the first time, information on the effect of an applied tensile load during such a test is provided. The consideration of the results is best divided into that of the case with applied external load and that without.

4.2.1 Zero External Load

According to an approximate calculation to be presented later, the reduction in ultimate strength and yield

strength for zero applied tensile load was at least an order of magnitude greater than would be estimated from a simple calculation of area reduction based on mean depth of penetration. A trend in this direction would be expected for the following reasons:

i) The cavitation damage increases the surface roughness very considerably (factor of about 25 in present tests, previously discussed), and this leads to numerous stress raisers. In addition, microcracks may significantly increase the effective penetration.

ii) In the present tests, the damage is not uniformly distributed around the perifery. Thus the actual tensile stress in the region of failure in the tensile machine may be considerably greater than the average stress in the plane of failure.

However, if the approximate penetration depth in the region of heaviest damage is observed from a photomicrograph as Figure 36-a, and it is assumed that this penetration is spread evenly over the surface, then, for the unstressed tests, the yield and breaking strength after exposure to cavitation are about as expected (C_1' of Table V to be explained later).

4.2.2 Applied External Load

As will be shown in an approximate calculation in the next section, the measured reduction in ultimate strength with applied load is greater than would be anticipated merely from the increase in mean depth of penetration with load. The same is true of yield strength (but not so substantially) as long as the external load is less than the proportional limit, so that

it does not cold-work the material. Possible mechanisms include at least the following:

i) Alteration of loading around a cavitation pit due to external load, as already discussed. In the present tests the external load was tensile, so, as previously indicated, the likelihood of local failure due to bubble implosions should be increased if these are caused by compressive stresses. The present data tends to indicate that this is the case. However, much more comprehensive data, including the effect of external compressive loading, is required to verify the above as well as the following mechanisms.

ii) An applied tensile load might be expected to increase the rate of propagation of microcracks, whereas the opposite would be expected from a compressive load. It would also seem reasonable that these would reduce the gross strength of the specimen by increasing the effective depth of penetration and providing stress-raisers, perhaps out of proportion to their effect upon weight loss.

iii) An applied tensile load might be expected to increase the likelihood of local fatigue failure from repeated relatively weak blows to the surface, whereas a compressive load would tend to inhibit such failures.

4.3 Approximate Models For Calculation

As a first crude approximation, it might be assumed that the tensile and yield strength of the specimen would be reduced in cavitation in proportion to the reduction in cross-sectional area as computed from the mean depth of penetration.

Then

$$S_f \quad to - 2(MDP) \quad (b) = P \qquad \text{- - - - - - - - - - - (1)}$$

where MDP -- b --- S_f --- P are defined below, or comparing a non-cavitated with a cavitated specimen, e.g., and assuming that the true failure stress is not changed:

$$\frac{P_2}{P_1} = \frac{to_2 - 2(MDP)_2}{to_1 - 2(MDP)_1} \qquad \text{- - - - - - - - - - - - - - - (2)}$$

Comparing the tensile strength of the unloaded but cavitated specimen to the mean for the non-cavitated specimens, e.g., the expected reduction in failure load becomes a factor of 0.98 . However, the observed reduction is 0.924.

For a better model, consider the sketch of a test specimen (Figure 40) and assume that the relation between maximum stress and load can be represented by

$$S_f \quad to - 2C_1(MDP) \quad C_2 = P \qquad \text{- - - - - - - - - - (3)}$$

where P = load applied by tensile test machine.

S_f = ultimate or yield stress depending on case considered.

C_1 = constant to be determined empirically, ratio of effective penetration to mean depth of penetration (MDP) calculated from weight loss.

$C_2 = C_3 b$

C_3 = constant for all specimens accounting for miscellaneous distribution and notch effects.

If the experimental results from two tests are compared, C_1 as it applies to these tests, can be computed. A sample calculation is shown in the Appendix.* The results

- -

* Full calculation in FGH Calculation File, 12/14/63.

are listed in Table V, and plotted in Figure 39 a and b.

TABLE V

EFFECTIVE MEAN DEPTH OF PENETRATION

Tests Compared	C_1	C_1'
1) Uncavitated to Zero Load Cavitated (Ultimate Strength)	4.69	0.844
2) Uncavitated to Max. Load Cavitated (Ultimate Strength)	7.19	4.52
3) Zero Load Cavitated to Max. Load Cavitated (Ultimate Strength)	25.10	1.285
4) Uncavitated to Zero Load Cavitated (Yield Strength)	5.46	.983
5) Uncavitated to Proportional Limit Load Cavitated (Yield Strength)	5.78	1.040
6) Zero Load Cavitated to Proportional Limit Load Cavitated (Yield Strength)	9.41	1.82

It is noted that the ratio (C_1) between the computed mean depth of penetration and its effective value, increases substantially with applied load. Possible reasons for this have already been discussed. The incremental effect in going from no load to full load is shown as well as the direct comparison between uncavitated and loaded and unloaded cavitated specimens.

C_1' (Table V) is analogous to C_1 except that it has been computed assuming the penetration in the regions of heaviest damage, as determined visually from a photomicrograph of a cross-section through such a region, is the mean depth of penetration. Since this determination cannot be very precise and the difference between appears small, it has been assumed for this

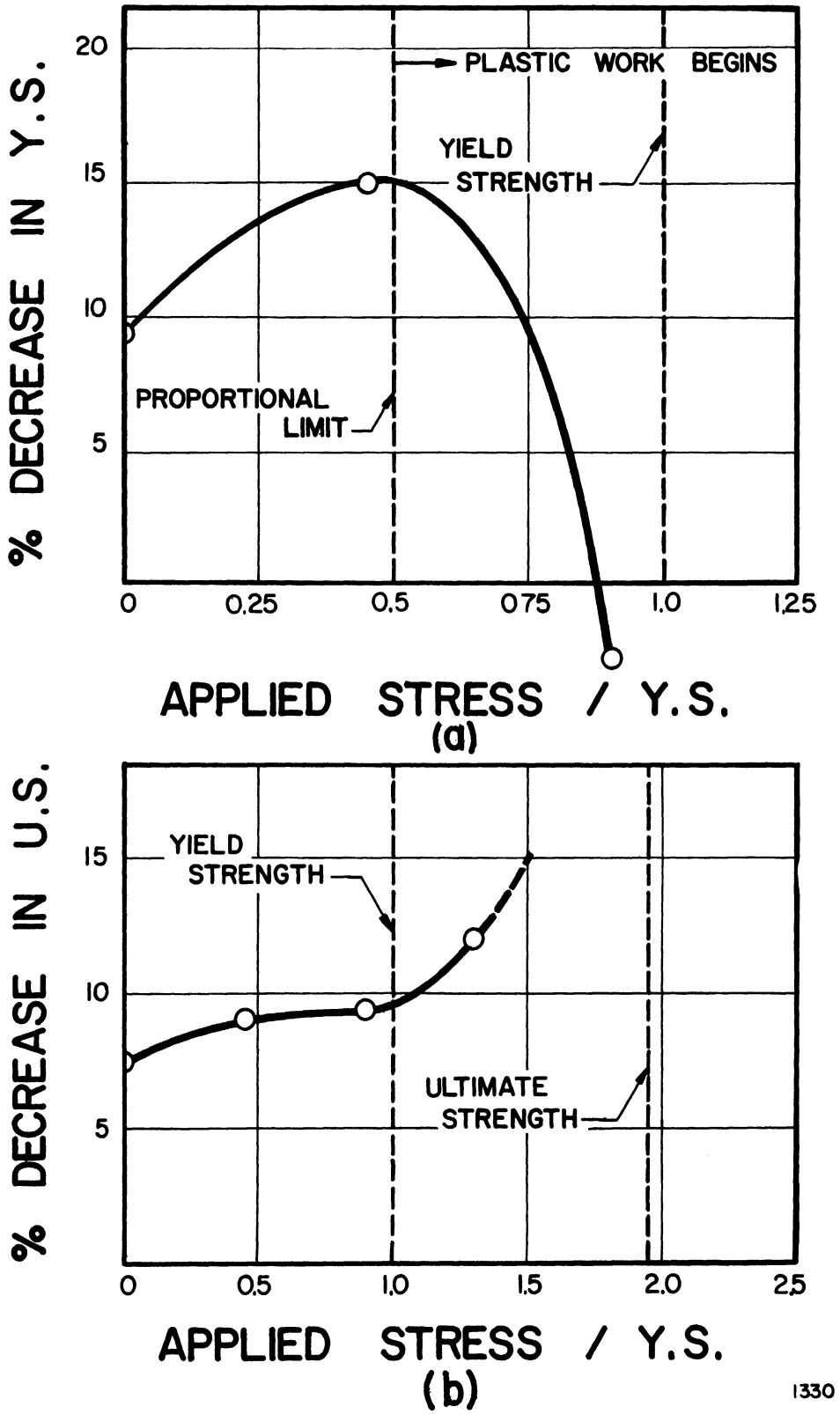

Figure 39 (a) Percent Decrease in Yield Strength vs. Applied Stress.
(b) Percent Decrease in Ultimate Strength vs. Applied Stress.

calculation that the ratio between mean depth of penetration and local penetration is the same for all the tests. It is noted that the values of C_1' for the unloaded tests are in both cases near unity, and also for the loaded tests involving yield strength, although there is a slight increase in C_1' with external load. However, for the loaded tests involving ultimate strength C_1' (as well as C_1) becomes substantially greater than unity, confirming the point previously made regarding the effect of external load.

An order of magnitude for a suitable multiplying factor to be used in computing the reduction in gross mechanical properties for cavitated structures can be obtained from Table V if estimates of either the mean depth of penetration over the involved area, or of the maximum depth of penetration, are available. The C_1' values show that a reasonably reliable estimate can be obtained from the latter if the component is essentially unstressed.

4.4 Miscellaneous Effects

4.4.1 Creep

Frequent checks were made throughout the tests to determine whether any load relaxation (i.e., creep), induced by the cavitation, had occurred. No large relaxation was observed. However, on two or three occasions with the specimen under maximum load (68,900 psi), there was a slight relaxation. The load was restored by applying, at most, a few hundred psi. No regular relaxation pattern was obtained, and the infrequent relaxations are believed due to initial sticking and subsequent

slippage of the specimen holder. Thus, apparently no creep of a "cold" specimen was observed in the cavitation facility, even for applied loads equal to about 1.3 times the yield strength.

4.4.2 Stress Corrosion

The possible effect of stress corrosion in the present tests is very difficult to ascertain, since only a small amount of inconclusive information in this area (mercury-stainless steel stress corrosion) is presently available in the literature. This problem could be explored by testing materials in cavitating mercury or water for which more definite applicable information is available.

5.0 CONCLUSIONS

The more important conclusions from the present investigation are:

1. The decrease in yield and ultimate strength due to known mean depths of penetration has been measured, as far as is known for the first time, for both stressed and unstressed specimens and found an order of magnitude greater than would be estimated from a direct calculation using cross-sectional areas based on mean depth of penetration. However, if the calculation is based on maximum depth of penetration as observed from a photomicrograph of a cross-section through the area of maximum damage, such a calculation gives reasonably approximate results.

2. The effect of an applied tensile stress (up to 1.3 times the yield strength) on the development of cavitation damage was small; the amount of damage usually, but not always,

being slightly greater for larger applied stresses.

3. An applied tensile stress (in combination with cavitation) caused a decrease in ultimate strength which increased monatomically and substantially as the applied tensile stress was increased. The amount of this increase was considerably more than would be expected from a consideration of mean depths of penetration.

4. An applied tensile stress, below the proportional limit, (in combination with cavitation) caused a decrease in yield strength. This decrease became larger for applied stresses up to about the proportional limit, but then it decreased, eventually becoming negative (i.e., yield strength increased) as the applied tensile stress approached the yield strength of the unstressed material.

5. No creep under cavitation was observed, even for applied stresses up to 1.3 times the yield.

6.0 LIST OF REFERENCES

1. Hammitt, F. G., et.al., "Fluid-Dynamic Performance of a Cavitating Venturi-Part II", Technical Report #3, ORA Project 03424, University of Michigan, December 1960.

2. Hammitt, F. G., "Observations on Cavitation Damage in a Flowing System", Trans. ASME, Jour. Basic Engr., Vol. 85, Series D, No. 3, September 1963.

3. Hammitt, F. G., et.al., "Cavitation Damage Tests With Water in a Cavitating Venturi", Technical Report #4, ORA Project 03424, University of Michigan, March 1962.

4. Hammitt, F. G., et.al., "Cavitation Damage With Mercury and Water in a Cavitating Venturi and Other Components", ORA Report No. 03424-9-T, Nuclear Engineering Department, University of Michigan, October 1963.

5. Ring, H. M., "Tension Tests", Memo Report, ORA Project 03424, University of Michigan, January 1963.

6. Barinka, L. L., and Hammitt, F. G., "Detailed Investigation of Cavitation Pitting Characteristics From Cavitating Venturi Tests", Technical Report #8, ORA Project 03424, University of Michigan, April 1963.

7. Hammitt, F. G., Barinka, L. L., McHugh, R. J., and Robinson, M. J., "Analysis of Hardness Indenter Pit Profiles", Internal Report #19, ORA Project 03424, University of Michigan, April 1963.

8. Hammitt, F. G., Barinka, L. L., Robinson, M. J., and McHugh, R. J., "On Transient Loading Effects in Cavitation Pitting", ASME Paper No. 63-WA-216 (Also, Internal Report #20, ORA Project 03424, University of Michigan, July 1963.

9. McLean, D., "Mechanical Properties of Metals", John Wiley & Sons, Inc., London, 1962.

10. Lipson, C. and Juvinall, R. C., "Application of Stress Analysis to Design and Metallurgy", Mechanical Engineering Department, University of Michigan, 1961.

11. Corten, H. T., and Dolan, T. J., "Cumulative Fatigue Damage", Paper presented at the International Conference on Fatigue of Metals, New York, November 1956.

APPENDIX

Derivation and Sample Calculation of Effective Penetration Relation

$$S_f \left[t_{o_i} - 2C_1 (MDP_i)\right] C_2 = P_i \quad \text{- - - - - - - - - (1)}$$

(symbols are as previously defined in report, and the index i refers to the particular run in question.)

Then, comparing two runs, it is possible to compute the multiplying constant $C_{1_{ij}}$, i.e.: as it exists between these conditions.

$$\frac{S_f \left[t_{o_i} - 2C_{1_{ij}} (MDP_i)\right] C_2}{S_f \left[t_{o_j} - 2C_{1_{ij}} (MDP_j)\right] C_2} = \frac{P_i}{P_j} \quad \text{- - - - - - - (2)}$$

where $i \neq j$

Then $P_j \left[t_{o_i} - 2C_{1_{ij}}(MDP_i)\right] = P_i \left[t_{o_j} - C_{1_{ij}}(MDP_j)\right]$

so $$C_{1_{ij}} = \frac{P_j(t_{o_i}) - P_i(t_{o_j})}{2\left[P_j(MDP)_i - P_i(MDP)_j\right]} \quad \text{- - - - - - - - - - (3)}$$

Apply this to the calculation of C_1 between cavitation under zero external load and maximum external load as it applies to ultimate strength.

Substituting numerical values from Table III into Eq. (3) :

$$C_1 = \frac{(94,761)(0.0232) - (90,055)(0.0227)}{2\left[(94,761)(270\text{x}10^{-6}) - (90,055)(250\text{x}10^{-6})\right]}$$

so $C_1 = 24.85$

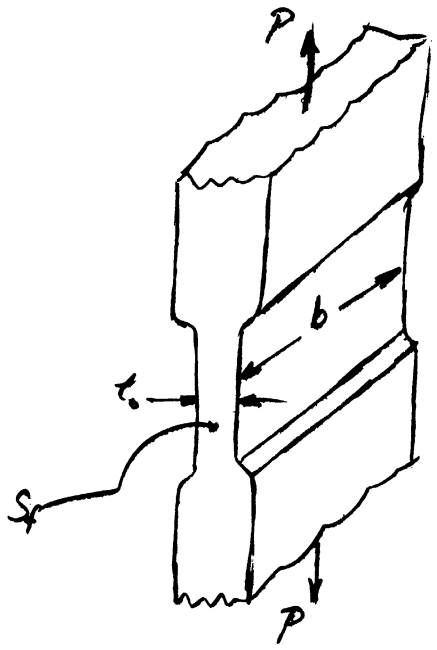

Figure 40

Sketch of Test Specimen For Calculation of C_1